Fault Ride-Through Capability of Doubly-Fed Induction Generators Based Wind Turbines

by

Abobkr Hamdia Abobkr

Submitted in partial fulfilment of the requirements
for the degree of Master of Applied Science

at

Dalhousie University
Halifax, Nova Scotia
March 2013

DALHOUSIE UNIVERSITY

DEPARTMENT OF ELECTRICAL AND COMPUTER ENGINEERING

The undersigned hereby certify that they have read and recommend to the Faculty of Graduate Studies for acceptance a thesis entitled "Fault Ride-Through Capability of Doubly-Fed Induction Generators Based Wind Turbines" by Abobkr Hamida Abobkr in partial fulfilment of the requirements for the degree of Master of Applied Science.

Dated: March 14,2013

Supervisor: _____

Readers: _____

_____

DALHOUSIE UNIVERSITY

DATE: March 14,2013

AUTHOR: Abobkr Hamida Abobkr

TITLE: Fault Ride-Through Capability of Doubly-Fed Induction Generators Based Wind Turbines

DEPARTMENT OR SCHOOL: Department of Electrical and Computer Engineering

DEGREE: MASc CONVOCATION: May YEAR: 2013

Permission is herewith granted to Dalhousie University to circulate and to have copied for non-commercial purposes, at its discretion, the above title upon the request of individuals or institutions. I understand that my thesis will be electronically available to the public.

The author reserves other publication rights, and neither the thesis nor extensive extracts from it may be printed or otherwise reproduced without the author's written permission.

The author attests that permission has been obtained for the use of any copyrighted material appearing in the thesis (other than the brief excerpts requiring only proper acknowledgement in scholarly writing), and that all such use is clearly acknowledged.

_____

Signature of Author

TABLE OF CONTENTS

LIST OF TABLES

LIST OF FIGURES

ABSTRACT

Due to growing concerns over climate change, more and more countries are looking to renewable energy sources to generate electricity. Therefore, wind turbines are increasing in popularity, along with doubly-fed induction machines (DFIGs) used in generation mode. Current grids codes require DFIGs to provide voltage support during a grid fault. The fault ride-through (FRT) capability of DFIGs is the focus of this thesis, in which modifications to the DFIG controller have been proposed to improve the FRT capability. The static synchronous compensator (STATCOM) controller has been applied with proposed method to study its influence on the voltage at the point of common coupling (PCC). The proposed method was also compared with other FRT capability improvement methods, including the conventional crowbar method. The simulation of the dynamic behaviour of DFIG-based wind turbines during grid fault is simulated using MATLAB/Simulink. The results obtained clearly demonstrate the efficacy of the proposed method.

LIST OF ABBREVIATIONS AND SYMBOLS USED

List of Abbreviations

ASGs	Adjustable speed generators
FSGs	Fixed speed generators
DFIG	Doubly fed induction generators
FRT	Fault ride through
LVRT	Low voltage ride through
E.On	German grid code
UK	National grid code
TSO	Transmission system operator
DSO	Disturbance system operator
SCIG	Squirrel cage induction generator
EMF	Electromotive force
RSC	Rotor side converter
GSC	Grid side converter
PCC	Point of common coupling
VSC	Voltage source converter
ESS	Energy storage system
FACTS	Flexible Ac transmissions system
UPFC	United power flow controller
STATCOM	Static synchronous compensation
PF	The power factor
EN 50160	The voltage disturbance standard

List of symbols

P_{mech}	The mechanical output power extracted from the wind
C_p	The performance coefficient
λ	The tip speed ratio
β	The pitch angle
ρ	The air density
A	The area covered by the rotor blades
v_{wind}	The wind speed
$v_{turbine}$	The turbine speed
K_p	The power gain
T_{elec}	The electromagnetic torque
T_m	The mechanical torque
H_{tot}	The total lumped inertia constant
w_{tr}	The turbine rotor angular speed
P_e	The electrical power
w_{g_mec}	The mechanical angular speed of the generator's rotor
w_{g_elc}	The electrical angular speed of the generator's rotor
V_s	The stator voltage
V_r	The rotor voltage
I_s	The stator current
I_r	The rotor current
R_S	The stator resistance
R_R	The rotor resistance
L_S	The stator leakage inductance
L_R	The rotor leakage inductance
L_m	The mutual inductance
E_r	The stator induced emf
E_r	The rotor induced emf
f_s	The stator frequency

f_r	The rotor frequency
p	The number of the pole pairs of the generator
s	The slip
w_s	The electrical stator angular velocity
w_r	The electrical rotor angular velocity
V_{ds}, I_{ds}	d-axis stator voltage and current
V_{qs}, I_{qs}	q-axis stator voltage and current
V_{dr}, I_{dr}	d-axis rotor voltage and current
V_{qr}, I_{qr}	q-axis rotor voltage and current
φ_{ds}	d-axis stator flux linkage
φ_{dr}	d-axis rotor flux linkage
φ_{qs}	q-axis stator flux linkage
φ_{qr}	q-axis rotor flux linkage
P_s, P_r	The stator rotor active power
P_g	The generated active power
Q_s, Q_r	The stator rotor reactive power
I_{dr_ref}	d-axis reference rotor current
I_{qr_ref}	q-axis reference rotor current
V_{pcc}	The voltage at the point of common coupling
$\mathrm{V_{G\_ref}}$	The reference voltage of DFIG
$\mathrm{V_{G\_mesu}}$	The measuring voltage at DFIG terminal
$\mathrm{X_s}$	The slop or drop reactance
$\mathrm{V_{STATCOM\_ref}}$	The reference voltage of the STATCOM controller
$\mathrm{V_{STATCOM\_mesu}}$	The measuring voltage at STATCOM terminal
$\Delta \mathrm{V_{ref}}$	The change of the reference voltage
γ	The impedance type factor
$\mathrm{i(t)}$	The fault current

ACKNOWLEDGMENTS

I thank God (ALLAH) for helping me in my research. I thank my lovely parents for their asking Allah to help me. I thank my brothers and my sister and all my family who pray for me, and I would thank my fiancee for her support ,and my friends here and back home in my country Libya for their support. I thank my supervisor, Dr. Mohamed El-Hawary for his guidance and advice.

CHAPTER 1 INTRODUCTION

1.1 MOTIVATION

Many of the world's governments have now openly acknowledged that the use of conventional energy sources is unsustainable due to environmental pollution and dwindling resources. With this recognition comes the search for better ways to implement alternative energy sources such as solar, hydroelectric and wind turbines. In addition to causing less environmental degradation, these alternative sources have several advantages. One advantage is that the prime mover's input, which is later converted to electricity, is renewable and thus will not run out. Moreover, there is an absence of waste products such as carbon dioxide, which occurs in coal-fired power stations, and renewable energy sources may require less maintenance than conventional sources.

Wind is by far the most popular renewable energy resources [1]. In 2012, a wind turbine and wind farm database of more than 50 countries around the world was published [2], showing the percentage of wind energy generated between 1997 and 2011, inclusive. China was the largest user of wind energy, with power generated exceeding 60 GW. In Libya, wind power generated 20 MW, and Canada was ranked ninth as a wind energy user, with a generation and production capacity of 5.265 GW. Figure 1.1 shows Canada's rise in wind energy production capacity from 1997 to the end of 2011.

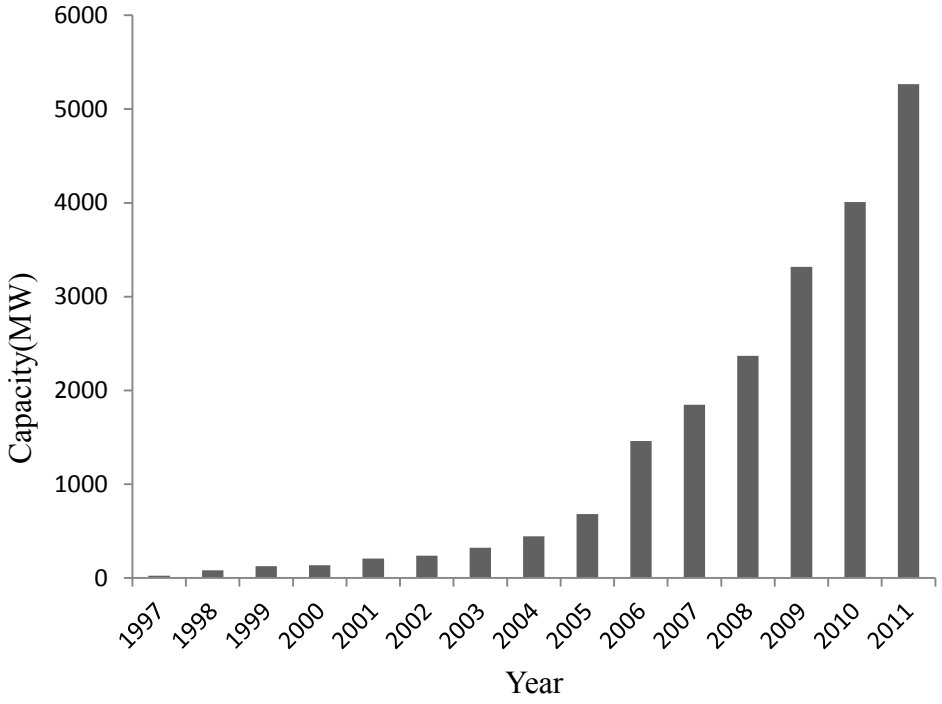

Figure 1.1 The power generated (MW) from wind each year in Canada [2]

Wind energy was first used to generate electrical power in 1887 by Charles Brush in Cleveland, USA. Brush used a DC generator with a battery to store the generated energy. In 1951, using an induction motor as a generator was discovered, but it was not until the 1970s, when the price of gas skyrocketed, that they were given a wider acceptance. As concerns over the environment grew through the 1980s and 1990s, so did the demand for renewable, sustainable and 'environmentally friendly' energy sources. By the 21st century, it was finally recognized that induction generators are among the best option to fulfill these requirements [3].

In the past, a simple squirrel-cage-induction generator-based wind turbines were directly connected to a three-phase power system and the rotor of the turbine was connected to the shaft of the generator through a fixed gear box. However, this type of

generator had to operate at a fixed wind speed, which is impractical and considered a disadvantage. In response to this limitation, some induction generators were developed to use pole-adjustable winding configurations in order to operate at variable wind speeds. Nowadays, many modern and large wind turbines use adjustable-speed generators (ASGs). Their main advantages over fixed-speed generators (FSGs) are that mechanical stress is reduced, power quality is improved, and system efficiency is higher. The most common type of ASGs used to produce electricity in wind turbines is the doubly-fed induction generator (DFIG) [4].

The most important advantages of using DFIGs coupled to wind turbines are:

- They provide a steady output voltage, including amplitude and frequency, regardless of wind speed and can thus be directly connected to the grid.
- The mechanical load stresses on wind turbines, which are produced during wind gusts, are reduced when using DFIGs. Additionally, during periods of low wind speeds, a DFIG maximizes the extracted energy (for details, see [4]).
- The possibility for independent control of active and reactive power due to smooth integration of wind turbine into the grid is achieved [5].
- Because only 25% to 30% of the power exchanged between a DFIG and the grid is completed through the power converter, the size of the power converter when using a DFIG is around one-quarter of the size of the power converter when three-phase synchronous generators are used. Thus, DFIGs lower the cost of the power converter [6].

The behaviour of DFIGs during grid disturbances like short-circuit faults has been the focus of numerous studies. In the past, the majority of national network operators did not

require that wind farms be connected to the grid during grid disturbances. However, due to an increase in wind farms, it is now mandatory for wind turbines to be connected to the grid during disturbances, in order to support it with reactive power [7]. Fault ride through (FRT) or low voltage ride through (LVRT) along with other methods and techniques have been developed to improve the FRT capability of DFIGs during fault periods.

1.2 THESIS OBJECTIVE AND CONTRIBUTION

As mentioned, numerous methods have been applied with the aim of improving the FRT capability of DFIGs. Examples include crowbar protection and reactive power sources in general. However, and as will be detailed in the next chapter, these methods have drawbacks. The key objective of this thesis is therefore to enhance the FRT associated with DFIGs during fault periods, improving the FRT requirement of voltage support during grid disturbances by reducing the voltage drop peak during fault periods. To this end, an external control circuit is proposed and applied to enhance FRT capability. Results obtained when using the proposed method will be compared to results obtained without this method as well as with those obtained by other techniques, including the crowbar method.

The idea for this work was derived from three theories. First, DFIG control is the key to DFIG performance during faults [8]. Second, the rotor side converter (RSC) controller can be modified to support grid voltage and, as a result, improve the FRT [9]. And third, the drop voltage is a function of a fault current [10]. These key theories will be discussed in detail later in this thesis.

The major contribution of this research work is proposing an improved FRT capability by modifying the RSC controller of the DFIG. The RSC controller is modified by

applying the external circuit so that the DFIG is able to support the grid voltage during grid fault and recovery.

With the intent of improving the FRT capability of DFIGs, a model of a wind turbine and drive train are presented and dynamic equation models of DFIGs are discussed and demonstrated.

1.3 THESIS OUTLINE

This thesis is organized in five chapters. The first chapter introduces the motivation behind this thesis as well as its objective and contributions. The second chapter reviews the literature and research area covered by this thesis. The third chapter discusses modeling of wind turbines and DFIGs and the behaviour of DFIG-based wind farms with AC grid connection during grid fault. This chapter also discusses some drawbacks of a specific method frequently used to improve the FRT capability of DFIG. Subsequently, this chapter explains the methodology and theory of this thesis and presents information on the origin of this method. In Chapter 4, the proposed method is applied to a DFIG-based wind turbine with power transmission system to check the validity of the presented method with regards to improving the FRT. Results obtained from the current research work are also compared to those obtained from other works. The final chapter provides the conclusion and some ideas for future work.

CHAPTER 2 LITERATURE REVIEW

This chapter briefly presents a literature review of the FRT capability of DFIG and the various methods that have been used, with varying success, to enhance the FRT issue.

2.1 FAULT RIDE THROUGH CAPABILITY OF DFIG WIND TURBINES

Fault ride through (FRT) or low voltage ride through (LVRT) can be defined as procedure may happen for an electric device or, in our case, a DFIG. Below are a few scenarios describing what should happen to an electric device during and after a voltage drop resulting from a load disturbance or other fault.

- The device should be disconnected from the AC grid temporarily until the dip disappears, after which the device should be reconnected.
- The device should never be disconnected from the grid and should remain constantly operational.
- The device should stay connected and act as a reactive power source to support the grid voltage.

Around the world, network operators issue grid codes, such as the German grid code (E.On) and the national grid code (UK). These grid codes determine which operational behaviour should occur or what action should be taken. Currently, according to the German grid code, wind turbines during a fault period (e.g., a short-circuit fault) must supply voltage support or reactive power support by increasing the provided reactive current to the grid [11]. In this case, implementation of the last of the three scenarios listed above is required.

As early wind turbines, some of which were coupled to a squirrel cage asynchronous machine, were very sensitive, the protection system disconnected the turbines even during minor disturbances. Nowadays, however, it should be a goal that wind turbines have the ability to continue operational through a fault and remain connected to the power system at all times [10].

Research indicates that the two most effective factors determining the FRT capability of DFIG wind turbines are converter control and converter protection system [8]. These two factors influence the performance of DFIGs during normal operation as well. Nevertheless, in [8], there is no information regarding voltage support recovery during a grid fault. During such an incidence, the voltage at the DFIG terminal dips down, causing a high transient rotor current due to the physical component of DFIG (namely, the magnetic coupling between the stator and the rotor, according to flux laws). Hence, during grid disturbances, stator disturbances are transmitted to the rotor [8].

To protect the rotor winding of DFIG and its converter circuits, a rotor over current protection called crowbar is applied [12] . The crowbar provides a safe route for the high transient rotor current by short circuiting the generator rotor windings, switching the crowbar to protect the rotor side converter (RSC) during faults.

Several principles and guidelines should be considered in designing crowbar protection [10]. Below are four key principles:

- First, keep the wind turbine connected.
- Second, prevent consumption of active power during a fault.
- Third, support the grid with reactive power during a fault and assist in voltage recovery.

- Fourth, enable a return to normal operation and steady-state condition quickly and efficiently.

From the principles listed above, we can conclude that the crowbar technique is a useful way to solve FRT capability. Not surprisingly, the crowbar method is considered the most popular of conventional techniques to improve the FRT capability of DFIG.

2.1.1 Crowbar Technique

In [13], a crowbar protection was applied using diodes and a thyristor in a series with a resistor. In [8], it was noted that FRT capability can be improved by using a proper value of crowbar resistance. Furthermore, to damp the torsional oscillation in the drive train caused by grid sag, a damping controller was applied to a thyristor crowbar.

A disadvantage of the crowbar protection method was presented in [14], where it was shown that, during a fault event, the controllability of a DFIG during the firing of the crowbar is lost because the DFIG will behave as a conventional squirrel cage induction generator (SCIG). Another drawback in using the crowbar method is stated in [15]. Since the stator during grid fault absorbs reactive power instead of supplying reactive power to the power network, two proposed methods have been implemented to prevent reactive power from being consumed. The aim of these two methods is derived from the principle of the theory of activation crowbar. The first method is to reduce the voltage value that operates the crowbar. To do this, an optimum value of a DC-chopper resistor is employed. In the second method, a strategy involving a grid side converter (GSC) controller is designed so that the main priority of GSC control is to compensate for the stator reactive power as well as support grid voltage recovery.

In contrast to conventional crowbar techniques, a fully controllable crowbar protection method was implemented in [16] to improve the FRT capability of the DFIG. It was controlled by the DC-link voltage. Another disadvantage of the crowbar method is that when the crowbar turns off and then, due to high rotor current or high voltage of the DC-link, attempts to turn back on, a two-phase fault can occur. This kind of fault causes a high negative-sequence voltage component in the stator winding, leading to a high rotor slip and inducing a high rotor voltage in the rotor winding. Consequently, the rotor current becomes difficult to control during this event until the fault has been cleared.

To solve the difficulties of controlling the rotor current, a new control method of the RSC, instead of using the crowbar method, was presented in [17]. However, some difficulties arose due to electromotive force (EMF) induced in the rotor that depended on negative-sequence voltage components in the stator-flux linkage and the rotor speed. The idea was based on eliminating undesired components in the stator-flux linkage by injecting the opposite components in the rotor current, with the intent to constrain the rotor current supplied to the RSC. This method, however, had limitations related to the control objective.

The differences between FRT with activated crowbar and with deactivated crowbar were introduced in [11]. According to the authors , the main disadvantage of using crowbar was the limitation of the reactive current provided from the DFIG during grid disturbances, which led to a limitation of voltage recovery support. Furthermore, the controllability of the DFIG during crowbar firing was lost because the DFIG will behave as a conventional squirrel cage induction generator.

2.1.2 Various FRT Capability Techniques

A protection scheme to enhance FRT capability was presented in [18]. In this work, instead of using the crowbar protection method during a fault condition, a supplementary dynamic resistor in a series with the RSC was applied. The advantages of using this method are reducing the disability time of RSC and reducing the torque fluctuation during protection time.

In [19] another technique aimed at improving the FRT capability of DFIGs without using the crowbar method, a scheme was proposed that uses a stator side series connected braking resistor, a DC-link chopper, and a coordinated control strategy of the DFIG. This scheme was designed to enable the RSC to remain connected during faults. As a result, the controllability during faults was maintained and the reactive power to support grid voltage recovery during grid faults was achieved. Moreover, by not using the crowbar protection option, stress on the turbine mechanical systems and specifically the torque fluctuation was significantly reduced. However, it was reported that the cost of using this scheme is high compared to the crowbar method. Other techniques can be applied to improving the FRT capability of DFIGs by connecting various reactive sources at specific locations.

In [11], shunt reactors and a capacitor were coupled to the best location, defined here as the point of common coupling (PCC), to generate the grid reactive power needed. Another location for connected reactive power sources to improve FRT capability is at the DFIG terminal, as proposed in [20]. In this research, it was applied by connecting an additional series-connected voltage source converter (VSC). Results obtained from this method demonstrated improved FRT capability compared to existing applied methods,

including the crowbar protection method. However, the method is considered more complicated, as it requires the use of three VSCs.

In [21], a comparison of different FRT solutions – namely, energy storage system (ESS) methods, the flux method and the crowbar method – was presented. The comparison evaluated the effects of the three different methods of FRT solutions under balanced and unbalanced faults, depending on wind turbine response. The results obtained demonstrated that, with the ESS method, it is not necessary to use the crowbar method, as the generator and converter continue to be connected and support the grid faults. However, this requires oversizing the RSC to hold out the high rotor current. Furthermore, the flux method was difficult to control, which can be observed from the oscillation at the voltage recovery. In contrast, the crowbar method provides operational stability, as can be noticed from the small transient at voltage recovery and the limitation of the rotor current obtained.

Kazi and Jayashri [9] proposed what seems to be a unique dynamic controller of solving and enhancing the FRT capability of DFIGs. A new modification of the RSC was applied by combining electromagnetic torque, current and voltage controller. Furthermore, the research modeled a flexible AC transmissions system (FACTS), one of the most widely used reactive power sources. Here, FACTS was used to generate and observe the reactive power required at the PCC. Subsequently, the proposed FACTS controller with FRT capability was compared to FRT capability with crowbar controller. It was reported that, when using the crowbar method, undesirable fluctuations of electromagnetic torque most likely occur. To solve this problem, FACTS was applied.

In [22], a novel scheme is proposed to help DFIGs remain connected to the power system and support voltage to the grid during unbalanced voltage or faults to assist voltage recovery. The concept of the research is that three single-phase converters can be used as an alternative to one three-phase converter.

2.2 SUMMARY

This chapter discussed various options for improving the FRT capability of DFIGs in order to stay connected to the power system network during fault conditions. As we saw, the most common method used is crowbar, but this method was revealed to have disadvantages such as loss of the controllability of DFIGs and their overconsumption of reactive power during grid faults. Consequently, the literature review presented some alternative methods to using the crowbar, citing their advantages and limitations. A few of these alternatives are using a resistor with RSC and connecting reactors and capacitors at the PCC.

CHAPTER 3 METHODOLOGY

3.1 INTRODUCTION

This chapter presents the methodology used to improve the FRT capability of DFIGs during faults. Specifically, it introduces the modification of the RSC of DFIGs by applying the proposed external circuit in order to enhance the FRT issue. In the next section, a classic configuration of a DFIG-based wind turbine is discussed prior to introducing the external circuit method.

3.2 THE CLASSIC CONFIGURATION OF A DFIG-BASED WIND TURBINE

In most instances, generating electricity from wind turbines is a two-stage process. In the first stage, the turbine rotor (prime mover) converts kinetic energy from the wind into mechanical rotational power. In the second stage, a generator converts mechanical power into electrical power. There are presently two options for coupling a turbine rotor to a generator shaft. One option, which is the most popular, involves coupling the two components physically via a gearbox. The other option is to connect the rotor directly to the generator. In the case considered, the type of generator is a DFIG, where the stator is directly connected to the grid and the rotor winding is connected to the grid via a back-to-back voltage source converter (BVSC). A common configuration of a DFIG-based wind turbine is illustrated in Figure 3.1. In the next section, a model of a wind turbine is introduced.

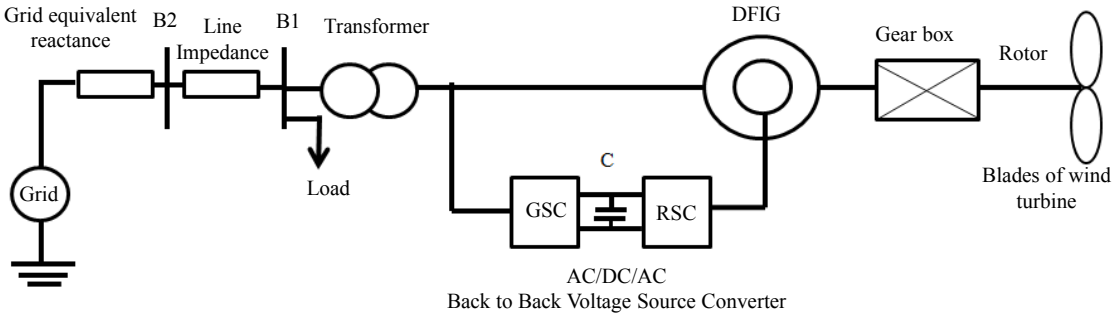

Figure 3.1 Conventional wind turbine configuration with a doubly-fed induction generator

3.3 MODELING OF WIND TURBINES

In modelling wind turbines, three basic components are taken into consideration: the turbine rotor, the gear box, and the generator shaft and electrical generator. These are defined as aerodynamic, mechanical and electrical components, respectively. The interaction between these three components is shown in Figure 3.2. In [23], it was determined that the amount of mechanical power that can be extracted from the wind by a turbine rotor depends on the dynamics of the wind (the aerodynamic component) and the response of wind turbine (the mechanical component). Hence, both the aerodynamic model and the mechanical model are required in wind turbine modeling.

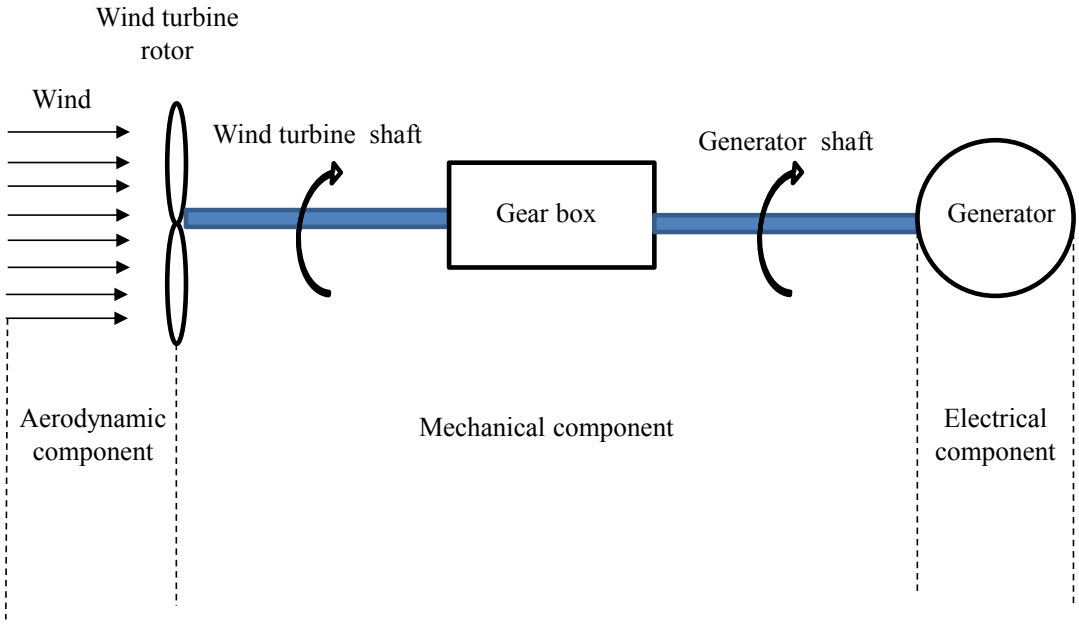

Figure 3.2 Basic wind turbine components

3.3.1 Aerodynamic Component Model

In a wind turbine simulation with FRT capability, it is desirable to involve the aerodynamic model during grid disturbances [12]. The aim of this model is to extract mechanical power from the wind by the rotor of the wind turbine, as mentioned in section 3.2. Equation (3-1) is referred to as a mechanical power equation [24, 25]. The magnitude of this equation depends on air density and wind velocity [1].

$$P_{mech} = C_p(\lambda, \beta)\frac{\rho A}{2} v_{wind}^3 \qquad (3\text{-}1)$$

where:

P_{mech} : the mechanical output power extracted from the wind, W

C_p : the performance coefficient or the power coefficient

λ : the tip speed ratio between turbine speed and wind

speed, $v_{turbine}/v_{wind}$

β : the pitch angle of the rotor blades, deg

ρ : the air density, Kg/m^3

A : the area covered by rotor blades, m^2

v_{wind}^3 : the wind speed, m/s

To simplify the computations, Equation (3-1) can be rewritten in the per unit system and calculated for specific values of ρ and A, using a power gain constant, as follows: [26]:

$$\mathrm{P_{mech}(pu)} = K_p C_p(pu) v_{wind}^3(\mathrm{pu}) \qquad (3\text{-}2)$$

where:

$\mathrm{P_{mech}(pu)}$: the power extracted from the wind in (pu) for the base power of specific values of ρ and A

$C_p(pu)$: the performance coefficient of the maximum value of C_p, in (pu), so that $C_p(pu) = C_p/C_p(base)$

K_p : power gain

v_{wind}^3 : the wind speed in pu, so that $v_{wind}(\mathrm{pu}) = v_{wind}/v_{base\ wind}$

The performance coefficient or the power coefficient (C_p) is considered as a characteristic of wind turbines. However, there are various methods to calculate C_p[12]. The next subsection presents these methods.

3.3.1.1 Calculation of the Performance Coefficient (C_p)

The performance coefficient $C_p(\lambda, \beta)$ is a function of the tip speed ratio λ and the pitch angle of the rotor blades β. During this research, three different methods were found [12, 24, 27].

1. Blade element method: in using this method, the calculation of C_p is considered difficult and complicated [27].
2. Look-up table method: the calculation of C_p is done using curves relating C_p versus λ, while β is a parameter.
3. Numerical approximations method: the relationship defining C_p is nonlinear; therefore, the numerical approximation is a perfect option to calculate C_p. This approximation has been improved in [24, 26], as follows:

$$C_p(\lambda, \beta) = 0.5176\left(\frac{116}{\lambda_i} - 0.4\beta - 5\right) * e^{\frac{-21}{\lambda_i}} + 0.0068\lambda \qquad (3\text{-}3)$$

where:

$$\frac{1}{\lambda_i} = \frac{1}{\lambda + 0.08 * \beta} - \frac{0.035}{\beta^3 + 1} \qquad (3\text{-}4)$$

The third method was employed in this thesis. Furthermore, by using Equations (3-3) and (3-4), the characteristics of wind turbines can be determined as will be explained later.

3.3.2 The Mechanical Component Model

The alternative name of the mechanical component model most widely used is a wind turbine rotor-generator drive train model [23]. The drive train consists of:

- wind turbine (WT) shaft
- gearbox
- generator shaft

The drive train model can be represented either by a two-mass or a one-mass system model [28]. If the one-mass model is utilized, the WT, gearbox and generator are lumped together into one equivalent mass. The following equation is known as the mechanical swing or motion equation. This equation models the drive train [29].

$$T_{elec} - T_m = H_{tot} \frac{dw_{tr}}{dt}$$

$$T_{elec} = \frac{\mathrm{P_e}}{w_{g\_mec}} \qquad (3\text{-}5)$$

$$T_m = \frac{\mathrm{P_{mech}}}{w_{tr}}$$

where:

T_{elec} : the electromagnetic torque

T_m : the mechanical torque

H_{tot} : the total lumped inertia constant

w_{tr} : the turbine rotor angular speed

$\mathrm{P_e}$: the electrical power

w_{g_mec} : the mechanical angular speed of the generator

Accordingly, and with [12, 30], Figure 3.2 has been expanded and developed into Figure 3.3, as follows.

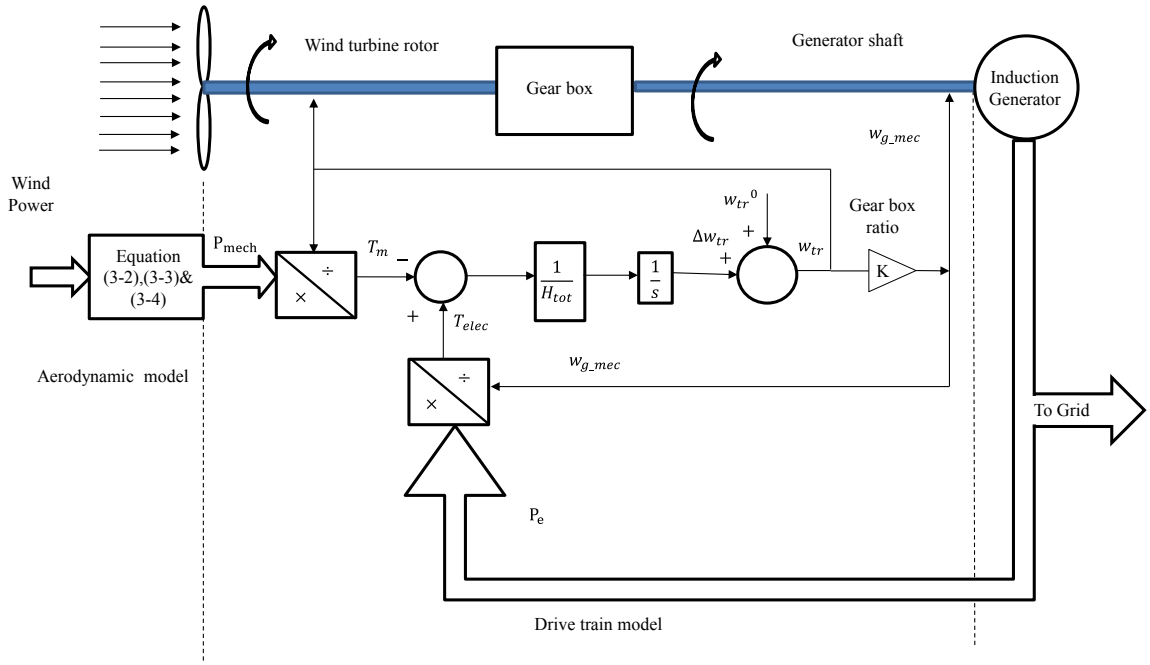

Figure 3.3 One-mass drive train representing the mechanical component

Figure 3.3 shows the three wind turbine components. Once the P_{mech} is calculated from the aerodynamic model, it will be fed to the drive train model. The objective of the drive train model is to calculate the w_{tr}, after which it is converted to w_{g_mech} by using the gear box ratio and subsequently delivers the w_{g_mech} to the generator. In the next section, an example of applying the aerodynamic and mechanical component equations in order to investigate the characteristics of a specific wind turbine is presented.

3.3.3 Wind Turbine Characteristics

The characteristics of any wind turbine may be defined as $P_{mech}(pu)$, as a function of WT- rotor speed $w_{tr}(pu)$ for different wind speeds as well as different pitch angles, β. Equations (3-2)(3-3)(3-4) are used for this purpose. A MATLAB program was written to draw the performance coefficient (c_p) as a function of tip speed ratio (λ), with pitch angle (β)as a parameter. As a result, the c_p (base) and λ(base) at $\beta = 0$ have been calculated as 0.4798 and 8, respectively, as shown in Figure 3.4.

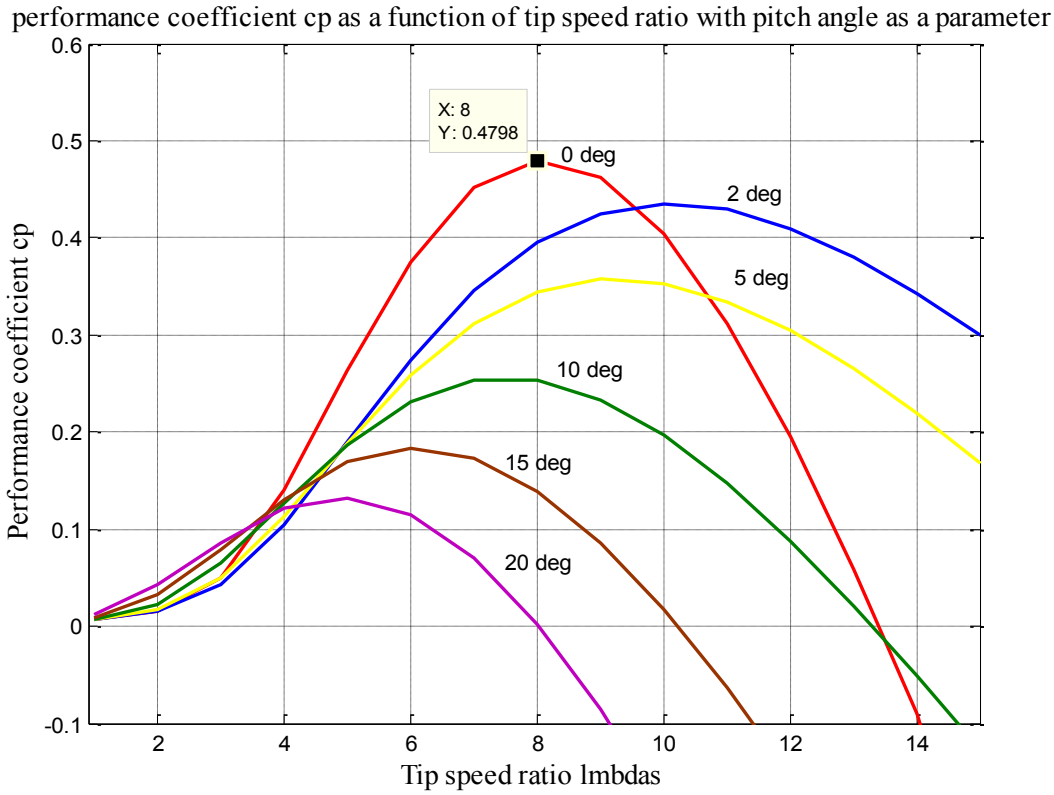

Figure 3.4 The performance coefficient Cp as a function of tip speed ratio λ, with pitch angle β as a parameter

Once the c_p (base) and λ (base) are calculated, they will be applied to the aerodynamic and mechanical models to find the relationship between P_{mech} (pu) VS $w_{tr}(pu)$. It is

should be noted that the WT rotor speed (w_{tr}) is referred to the generator side [1, 26], so that:

$$w_{tr} \text{ (referred to as the generator)} = \frac{w_{tr}\,(pu)}{w_{g\_mec}(pu)} \qquad (3\text{-}6)$$

where:

$w_{g\_mec}(pu)$: the base of the mechanical angular generator speed (constant) ,pu

In this thesis, and unlike the conventional simulations which use the wind turbine block in the MATLAB /SIMULINK library, a block was modeled by supplementing the drive train subsystem with assumption of $T_{elec} = 0.8$ pu and H_{tot} =3.5. In this example, 12(m/s) base wind speed,k_p at this base wind speed= 0.73 pu, $\beta = o$ and w_{g_mec}=1.2 (pu) have been implemented using MATLAB /SIMULINK. These values have been taken from [26], for the wind speeds 14, 13.2, 12, 10.8, 9.6, 8.4, 7.2 and 6 m/s. The MATLAB program illustrated in Figure 3.4 is given in Appendix A, while the wind turbine characteristics methodology is summarized in the flowchart Figure 3.5, the Simulink file is shown in Figure 3.6, and the wind turbine characteristics are illustrated in Figure 3.7.

The aim of the characteristics of any wind turbine is to provide an expectation of how to design the generator's control system in order to track these characteristics and extract maximum power from the wind.

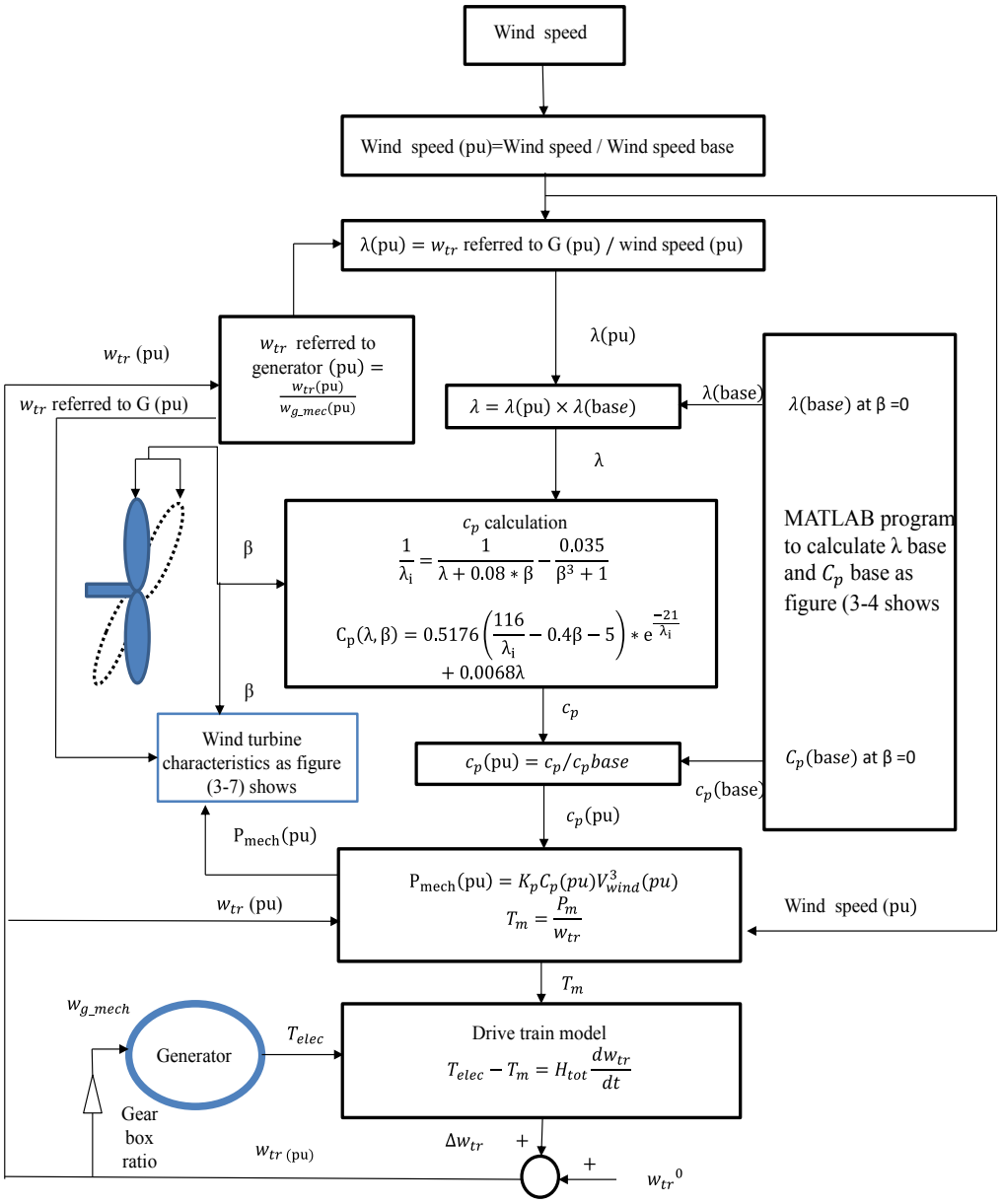

Figure 3.5 Flowchart of the methodology of a wind turbine

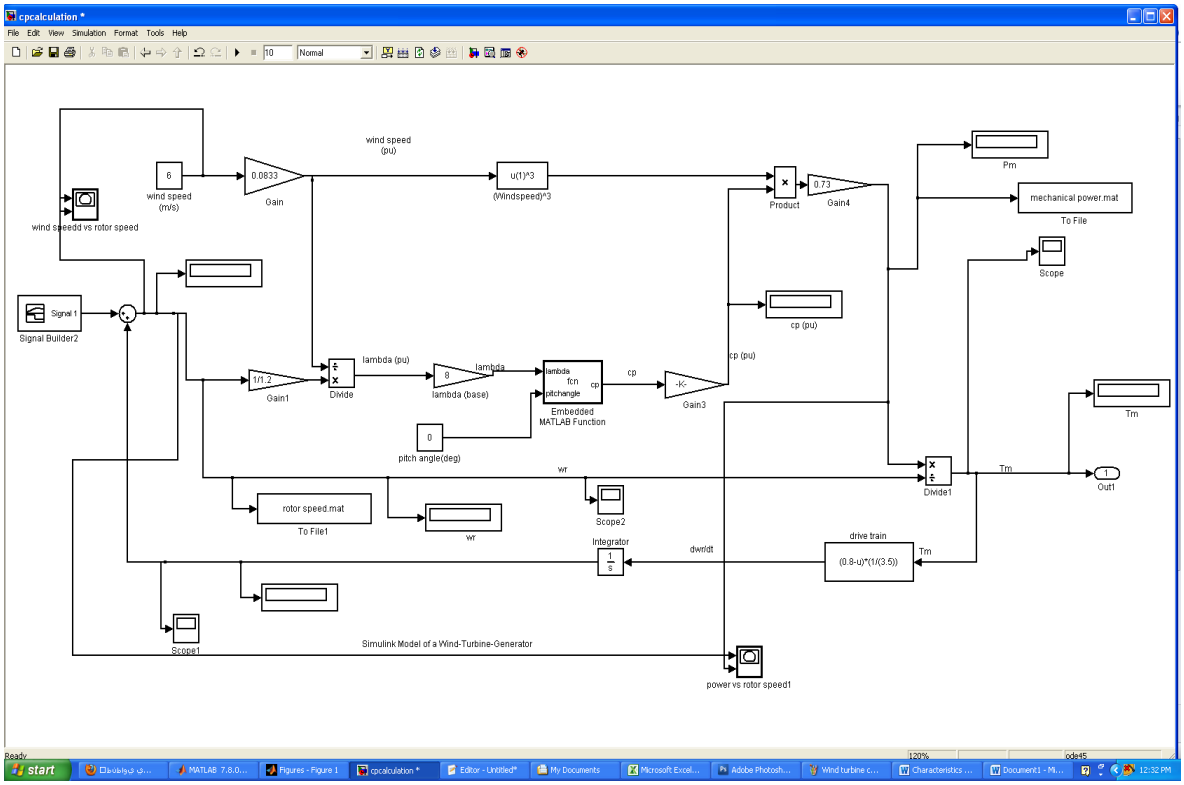

Figure 3.6 MATLAB/SIMULINK of a wind turbine with drive train

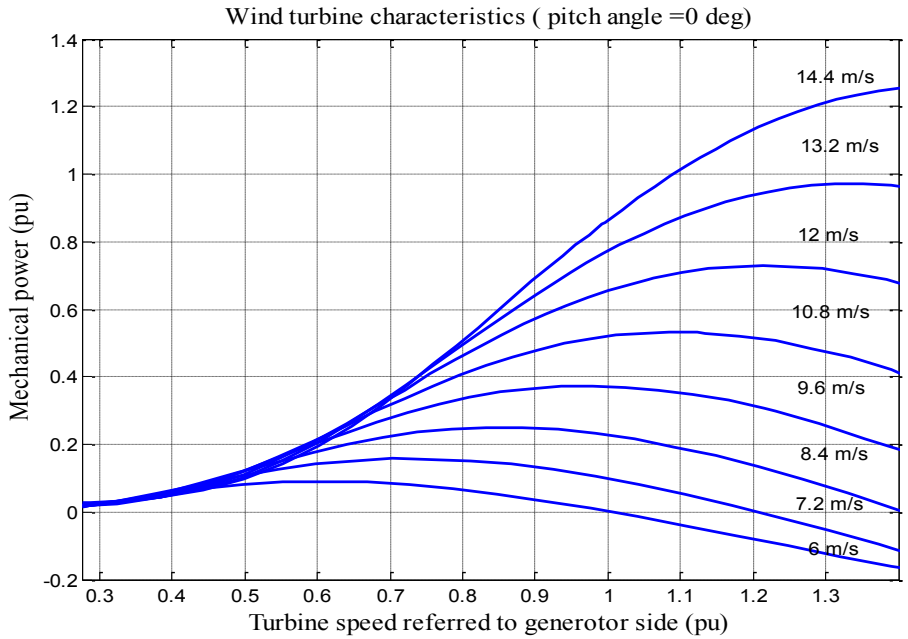

Figure 3.7 The wind turbine characteristics at β=0

3.3.4 Model of DFIG System

Double-fed induction generators are preferable in wind turbine applications that require a constant output power system frequency at various speeds of the generator shaft. DFIGs are electric generators that have windings on both stator and rotor sides. The stator is directly connected to the grid and the rotor is connected to the grid via a power converter, as shown in Figure 3.1. Furthermore, the voltage on the stator is supplied from the power system and the voltage on the rotor is induced by the power converter, the generated electrical power is supplied to the grid through both the stator and the rotor. The DFIG has three inputs: the stator voltage (V_s), the rotor voltage(V_r), and the mechanical angular speed of the generator's rotor (w_{g_mec}). It also has three outputs: the induced stator(I_s), the rotor currents(I_r), and the electromagnetic torque (T_{elec}), as shown in Figure 3.8. The next sections provide a brief description of DFIG theory and equations.

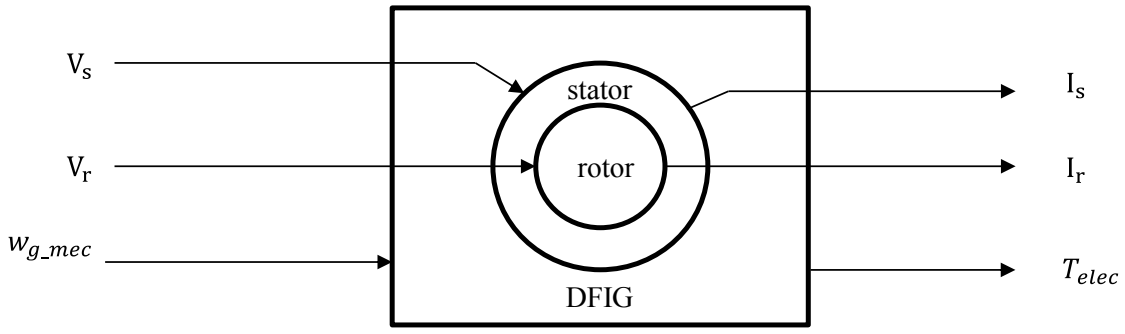

Figure 3.8 DFIG block with inputs and outputs

3.3.4.1 The Basic Concept of DFIG

As illustrated in Figure 3.8, when the stator is supplied by the grid voltage V_s of frequencyf_s, the stator flux is induced and will rotate at a constant speed, which is known as synchronous speed (n_s). Consequently, and according to Faraday's law, the stator flux will induce an electromotive force in the rotor windings (EMF_r). This, together with the injected voltage from the power converter to the rotor windings (V_r), will induce the rotor current, I_r, which also produces a rotating rotor flux. Similarly, this rotating rotor flux will induce the electromotive force in the stator windings (EMF_s), which induces a current in the stator windings, I_s. The equivalent circuit for steady state of DFIG is illustrated in Figure 3.9.

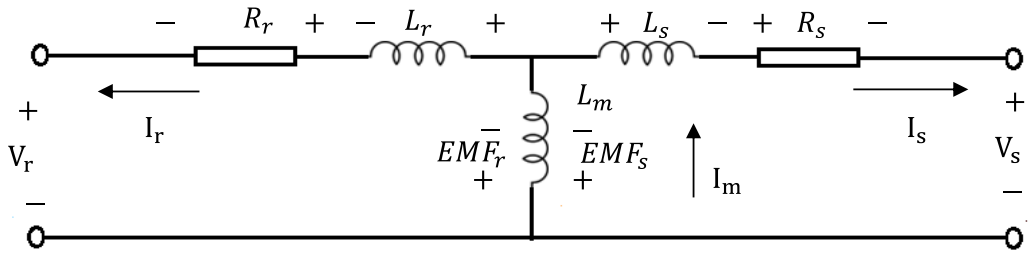

Figure 3.9 One-phase equivalent circuit for steady state of DFIG [30]

Where:

R_s R_r : the stator, rotor resistance

L_s L_r : the stator, rotor leakage inductance

L_m : the mutual inductance

I_s I_r : the stator, rotor-induced current

EMF_S EMF_r : the stator, rotor electromotive force induced

The voltages and currents in the rotor windings rotate at a speed which is known as the electrical rotor angular velocity(w_r). Likewise, the voltages and currents in the stator windings rotate at the electrical stator angular velocity (w_s). The relation between w_r and w_s is given as follows:

$$w_r = w_s - w_{g\_elc}$$
$$w_{g\_elc} = w_{g\_mec} \times p \quad (3\text{-}7)$$

where:

w_{g_elc} : the electrical angular speed of the generator's rotor

p : the number of the generator's pole pairs

In addition, the relation between w_s and w_{g_elc} is commonly called the slip (s). By combining this relation with Equation (3-8), the relation between w_s and w_r is expressed in Equation (3-9)

$$\text{slip (s)} = \frac{w_s - w_{g\_elc}}{w_s} \quad (3\text{-}8)$$

$$w_r = sw_s$$
$$f_r = sf_s \quad (3\text{-}9)$$

Where

f_r , f_s the stator, rotor frequency

The sign of the slip determines the mode of the DFIG operation, either in a sub-synchronous operation or hyper-synchronous operation, as well as the receiving or supplying the power, as shown in Figure 3.10.

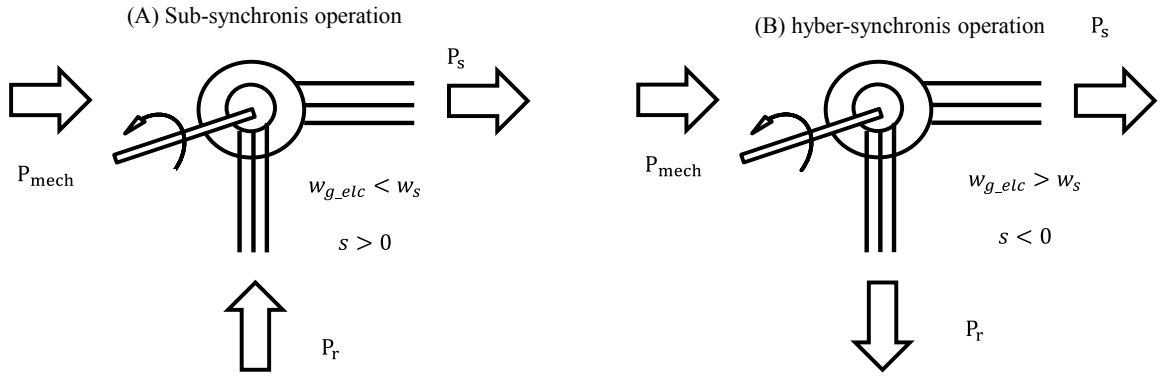

Figure 3.10 Active power flow of DFIG at different modes of operation according to the slip sign

According to various models of DFIGs established by numerous authors, the space vectors of the machine are represented by different reference frames in order to create a dynamic model of a DFIG. Examples of these frames are the stator reference frame (α, β), the rotor reference frame (D, Q), and the synchronous reference frame $(d.q)$. It should be noted that the difference between these reference frames is the rotating speed of the frame, where the speeds are zero (stationary), the electrical angular speed of the generator's rotor (w_{g_elc}) and synchronous $(n_s \text{or } \mathrm{w_s})$ of the given frames respectively. To achieve an independent control of the active and reactive power and to simplify the model of DFIG by eliminating the zero sequence components, the direct and quadrature rotating axis (d, q) reference frame has been frequently implemented to model the DFIG.

3.3.4.2 dq Reference Frame

Over the course of researching this thesis, many studies aimed at modeling the DFIG in dq reference were analyzed [7, 27-33]. The main difference between the models were the signs. Some were modeled as a general machine (the signs of the currents I_s and I_r are identical and indicate that the currents flow toward the machine), unlike Figure 3.9 [31-33], while other models were designed as a generator (the signs of the I_s and I_r are opposite, where I_s flows toward the grid) [7, 28] or established as a generator (the signs of the I_s and I_r are similar, where I_s and I_r flow toward the grid), as shown in Figure 3.8 [27, 29]. However, even between [29] and [27] there is a difference, but not in the current signs. Instead, the difference is in the polarity of the voltage, which is induced by a changing flux. Therefore, to find an acceptable model of a DFIG, mathematical and electrical laws have been applied.

- First, a stator and rotor flux linkage (φ_s, φ_r)will be produced by the stator and rotor induced currents (I_s, I_r), respectively. By a change in the flux linkage, the polarity of the induced voltage opposes the current which produces it (Lenz's law).
- Second, a transformation matrix is applied to the traditional a, b, c model to switch to the dq reference frame. As a result, Figure 3.9 will be devolved to Figure 3.11. Furthermore, from Figure 3.11, it can be observed that, the polarities of the induced $w_s\varphi_{dqs}$ and $sw_s\varphi_{dqr}$ voltages which are induced by the change of the flux linkage $\frac{d}{dt}\varphi_{dqs}$ and $\frac{d}{dt}\varphi_{dqr}$ will oppose the polarities of the I_{dqs} and I_{dqr}, respectively .

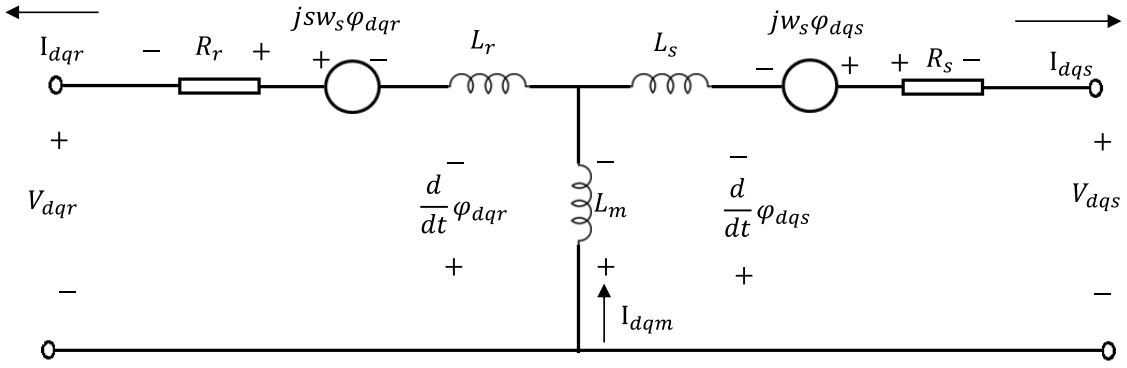

Figure 3.11 The dq model of DFIG

- Third, applying the Kirchhoff voltage law to Figure 3.11 will give:

$$V_{dqs} = -I_{dqs}R_s + jw_s\varphi_{dqs} - \frac{d}{dt}\varphi_{dqs}$$
$$V_{dqr} = -I_{dqr}R_r + jsw_s\varphi_{dqr} - \frac{d}{dt}\varphi_{dqr} \quad (3\text{-}10)$$

- Fourth, applying the pharos notation theory to simplify, the dq reference frame can by expressed as follows:

$$\overrightarrow{x_{dq}} = x_d + jx_q$$
$$\overrightarrow{x_{dq}} = \begin{bmatrix} x_d \\ x_q \end{bmatrix} \quad (3\text{-}11)$$

Hence:

$$jw_s\varphi_{dqs} = jw_s(\varphi_{ds} + j\varphi_{qs}) \quad (3\text{-}12)$$

$$jw_s\varphi_{dqs} = jw_s\varphi_{ds} - w_s\varphi_{qs}$$

$$jw_s\varphi_{dqs} = \begin{bmatrix} -w_s\varphi_{qs} \\ w_s\varphi_{ds} \end{bmatrix}$$

In a similar way, in V_{dqr}

$$jsw_s\varphi_{dqr} = \begin{bmatrix} -sw_s\varphi_{qr} \\ sw_s\varphi_{dr} \end{bmatrix} \quad (3\text{-}13)$$

By substituting Equations (3-8) (3-12) and (3-13) into (3-10), the stator and rotor phase of DFIG in the dq reference frame can be expressed according to the following equations:

$$\begin{aligned} V_{ds} &= -R_s I_{ds} - \frac{d}{dt}\varphi_{ds} - w_s\varphi_{qs} \\ V_{qs} &= -R_s I_{qs} - \frac{d}{dt}\varphi_{qs} + w_s\varphi_{ds} \end{aligned} \quad (3\text{-}14)$$

$$\begin{aligned} V_{dr} &= -R_r I_{dr} - \frac{d}{dt}\varphi_{dr} - (w_s - w_{g_{elc}})\varphi_{qr} \\ V_{qr} &= -R_r I_{qr} - \frac{d}{dt}\varphi_{qr} + (w_s - w_{g_{elc}})\varphi_{dr} \end{aligned} \quad (3\text{-}15)$$

where:

$$\varphi_{ds} = L_s I_{ds} + L_m I_{dr} \quad (3\text{-}16)$$

$$\varphi_{qs} = L_s I_{qs} + L_m I_{qr}$$

$$\varphi_{dr} = L_r I_{dr} + L_m I_{ds}$$

$$\varphi_{qr} = L_r I_{qr} + L_m I_{qs}$$

where:

V_{ds}, I_{ds}	d-axis stator voltage and current
V_{qs}, I_{qs}	q-axis stator voltage and current
V_{dr}, I_{dr}	d-axis rotor voltage and current
V_{qr}, I_{qr}	q-axis rotor voltage and current
φ_{ds}	d-axis stator flux linkage
φ_{dr}	d-axis rotor flux linkage
φ_{qs}	q-axis stator flux linkage
φ_{qr}	q-axis rotor flux linkage

It should be noted that Equations (3-14), (3-15) and (3-5) represent the DFIG as a fifth-order model. Also, DFIG can be represented as a third-order model when the stator transients (i.e., the differential term in Equations (3-14)) are left out, which increases the computation speed in power system simulation software [27, 32]. In [34], a first-order model was given by leaving out the rotor transient. It should also be mentioned that the demonstrated equation of the DFIG dynamic model (3-14)(3-15) are also given in [29].

The active power of the stator (P_s), rotor (P_r), generated power (P_g) and electromagnetic torque (T_{elec}) are calculated as:

$$P_s = \frac{3}{2}\left(V_{ds}I_{ds} + V_{qs}I_{qs}\right)$$

$$P_r = \frac{3}{2}\left(V_{dr}I_{dr} + V_{qr}I_{qr}\right) \quad (3\text{-}17)$$

$$P_g = P_s + P_r$$

$$T_{elec} = L_m(I_{qs}I_{dr} - I_{ds}I_{qr})$$

The reactive power of the stator (Q_s), rotor (Q_r) and generated power (Q_g) are calculated as:

$$Q_s = \frac{3}{2}\left(V_{qs}I_{ds} - V_{ds}I_{qs}\right)$$

$$Q_r = \frac{3}{2}\left(V_{qr}I_{dr} - V_{dr}I_{qr}\right) \quad (3\text{-}18)$$

$$Q_g = Q_s + Q_r$$

3.3.5 Back-to-Back Voltage Source Converter

As mentioned earlier in this chapter, the stator and rotor circuits have different frequencies. In general, the stator frequency(f_s) is fixed if the stator is connected directly to the grid, which means that the V_s is fixed. In contrast, the V_r will supply via the voltage source converter, which allows for a modification of the V_r. Hence, the rotor frequency(f_r) is variable and depends on the w_{g_elc}, according to Equations (3-8) (3-9). This injected rotor voltage V_r (which means w_r) must be at an appropriate value so that $w_{g_elc}$is equal to its reference value, allowing the DFIG to extract the maximum amount of P_{mech} from the wind turbine.

In general, it is possible to conclude that a relation between w_{g_elc} and the power generated by DFIG exists. In fact, a relation between I_r and the generated stator power P_s and Q_s is present. In other words, the I_r is controlled and traces its reference value to achieve the optimum value of the P_s and Q_s. Furthermore, by applying a dq reference frame in a specific way, the stator's active and reactive power can be controlled independently so that I_{qr}, I_{dr} control the P_s and Q_s, respectively.

As is known, there are a many of different types of controllers. The one most extensively used is the proportional-integral (PI) controller. It is possible to insert the input of (PI) as a current while the output of (PI) as a voltage by means of using the proper proportional-integral parameters of (PI). Moreover, the relation between the current and the voltage is transformed to transfer function using Laplace domain [35]. This controller is called the rotor-side converter (RSC) control. Once the reference rotor currents I_{dr_ref}, I_{qr_ref} are calculated and inserted into the PI controller, the voltages V_{dr}, V_{qr} are obtained. These will be injected into the DFIG via the rotor-side converter (RSC).

The other part of the two-level converter (AC/DC/AC) is known as the grid-side converter (GSC). A DC-link separates the RSC and GSC, as shown in Figure 3.1. The aim of the GSC is to maintain the DC-link voltage (V_{dc}) as a constant. It is noteworthy to mention that the major part of the clarification presented in sections 3.3.4 and 3.3.5 are derived from [10].

3.4 DOUBLY-FED INDUCTION GENERATOR DURING FAULTS

In the past, the majority of grid operators did not require that wind farms be connected to the grid during grid faults. However, at present, due to an increase in the implementation of wind turbines, keeping wind turbines connected during grid faults has become mandatory. Moreover, during grid faults, wind turbines have to supply voltage support or reactive support. These two requirements are called fault-ride through (FRT).

3.4.1 Reactive Power Support by DFIG

Reactive power or voltage support is requested during grid faults by increasing the reactive current provided to the grid in order to support the grid voltage.

Reactive power control (supply or consumption) as a function of the voltage at the point of common coupling between the DFIG and the grid (PCC) is defined in grid codes, which are issued by the transition system operators (TSOs). It should be noted that, due to the difference between grid structures, the definition may vary from company to company. For instance, Figure 3.12 shows the relation between the reactive power control of DFIG and the voltage at PCC in a German grid code (E. On) [11].

From Figure 3.12, it can be concluded that, when the voltage at the PCC decreases below a specific range, the DFIG would act as a reactive power source (e.g., as capacitive) and supply reactive power to the grid in order to increase the voltage. Furthermore, the DFIG would turn into over-excited mode. On the other hand, if the voltage at the PCC increases to a level above a specific range, the DFIG would act as an inductive load and consume reactive power in order to decreases the voltage. In this case, the DFIG would operate in under-excited mode, as illustrated in Figure 3.12 [10].

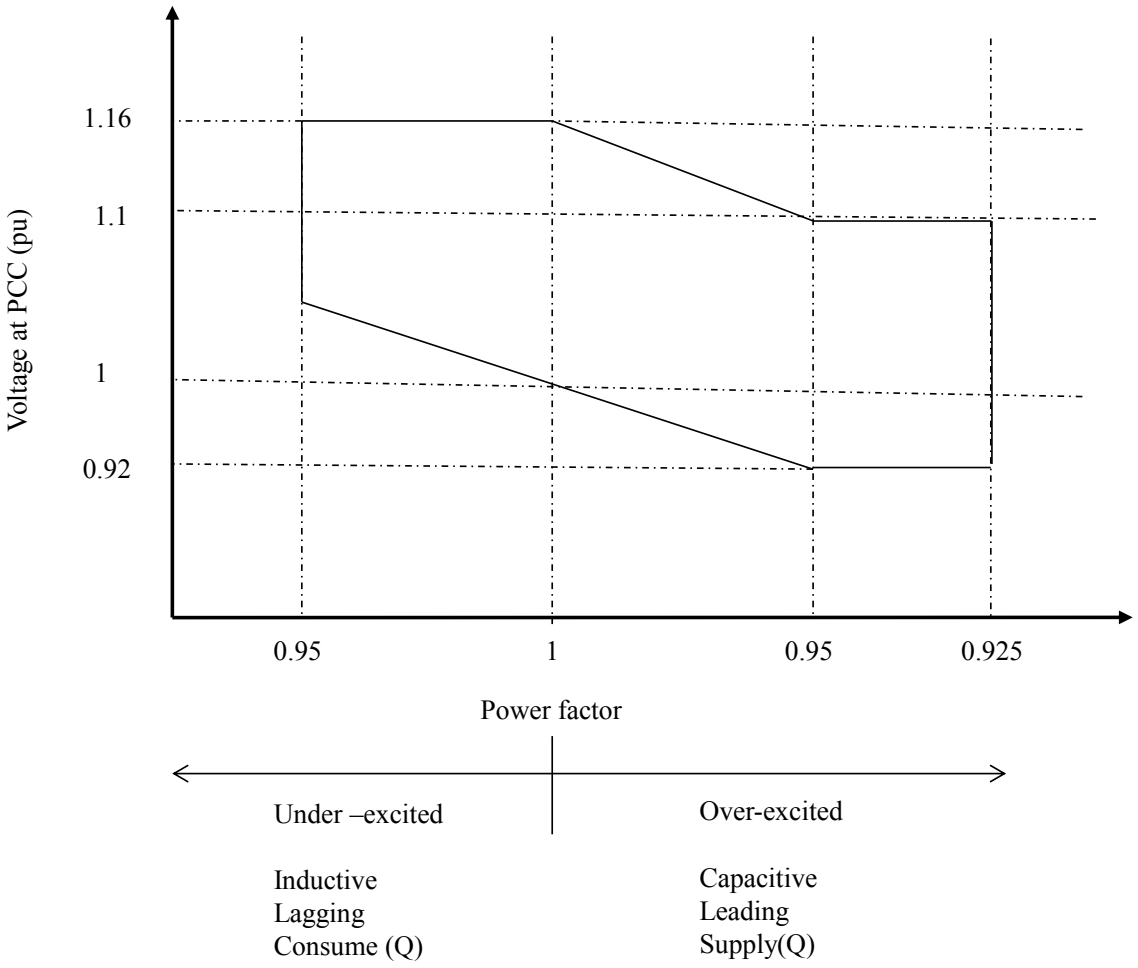

Figure 3.12 The reactive power control as a function of the voltage at PCC in (E.On)

Commonly, the reactive power sign depends on DFIG conditions. So, if the DFIG is in over-excited mode, the reactive power(Q) is labelled positive. Conversely, if the DFIG is in under-excited mode, the reactive power (Q) is labelled negative. The (P-Q) characteristics of a DFIG are shown in Figure 3.13.

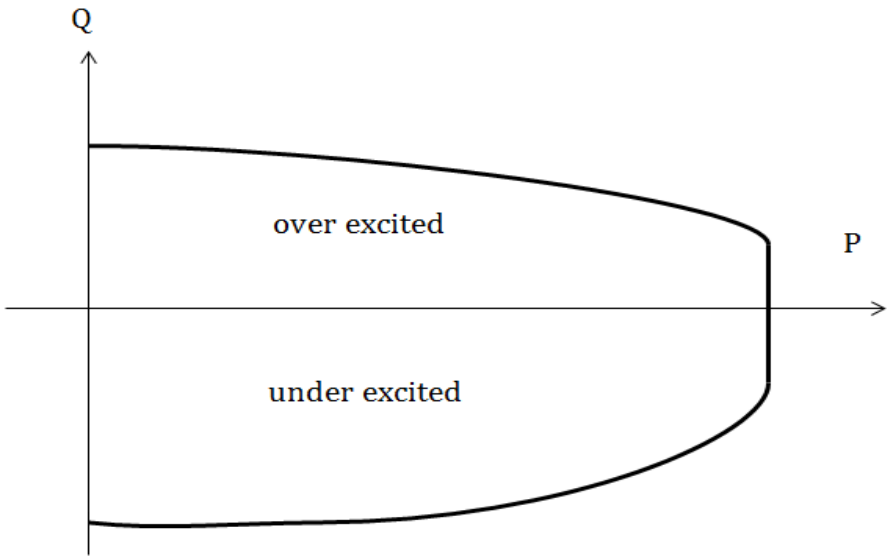

Figure 3.13 P-Q characteristics of a DFIG

According to [11] and Figure 3.13, three advantages of a DFIG as a reactive power source can be concluded as follows:

- Firstly, the DFIG can provide reactive power (Q) even though no active power(P) is generated.
- Secondly, the DFIG can supply more reactive power in under-excited mode than in over-excited mode.
- Thirdly, the DFIG has the ability to operate at all four quadrants of the complex plan. Consequently, the DFIG becomes a preferable reactive power source (VAr) for the grid requirements, especially during faults.

Therefore, during grid faults, the DFIG can supply reactive power during transient situations, including faults. This is the key focus of the present thesis and will be discussed in the next section.

Even more specifically, DFIG-based wind turbines have to support the grid voltage by injecting additional reactive current. For this purpose, the voltage control must be stimulated (as shown in Figure 3.14) so that during faults and when the voltage dips more than 10%, the voltage control can supply reactive current within 20 (ms) after the fault is realized. Subsequently, for each 1% of the voltage dip, at least 2% of the rated reactive current is supplied. For instance, it should supply at least 0.5(pu) reactive current any time the voltage dips under 25% due to grid disturbances or when the dead band around the rated voltage of 10% $(V_{max} = 1.1\,V_N, V_{min} = 0.9V_N)$ is allowed, as illustrated in Figure 3.14 [36].

In addition, grid codes nowadays demand a standard for successful FRT of wind turbines, requesting that voltage support be at least up to 15% rating voltage [14].

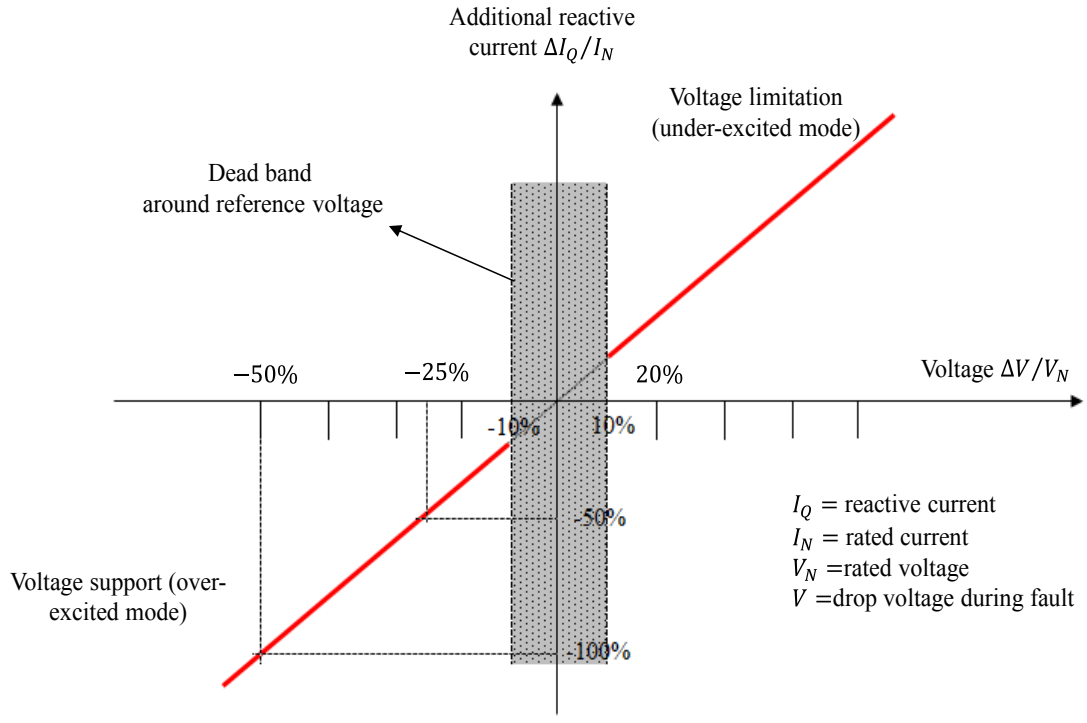

Figure 3.14 Characteristics of wind turbine voltage control [36]

In general, only 30% of power is exchanged through the power converter between the DFIG and the grid. Consequently, the required size of the converter is only about 30% of the full-power converter, and thus DFIGs are considered as non-full-power converters [6]. In fact, non-full-power converters such as DFIGs are more sensitive to grid faults than full-power converters and therefore require protection. Over-current protection, called crowbar protection, is commonly used [8]. As mentioned in Chapter 2, crowbar protection is considered an FRT capability method and has many disadvantages, as summarized below:

1. During faults and crowbar activation, the controllability of DFIG is lost because the DFIG would behave as a squirrel cage induction generator [14].
2. During faults and crowbar activation, the stator of DFIG observes reactive power instead of providing reactive power and voltage support to the grid [15].
3. Due to the high sensitivity of a crowbar to any case of a high rotor current or a high voltage of the DC-link, repeatedly turning the crowbar circuit on and off causes a high negative voltage component in the stator. This in turn causes a high rotor slip, which induces a high rotor voltage in the rotor. Consequently, the controllability of the rotor current during this event becomes difficult [16].
4. During faults and crowbar activation, the reactive current provided from DFIG to support the grid voltage is limited [11].

Because of these drawbacks and also because the majority of modern wind turbines coupled to DFIG attempt to ride through the faults (FRT) without switching on the crowbar [11], difficulties arise. Consequently, in this thesis, an alternative method to improve the FRT instead of the crowbar method is proposed. However, as any new

proposed method for solving the FRT has to be compared to the conventional FRT method (i.e., crowbar protection), a comparison between the crowbar method and the proposed method is thus the scope of the present thesis.

Voltage dips or sags are the most common grid disturbances. Voltage dips are defined as a reduction in voltage from tens of milliseconds to hundreds of milliseconds. According to the voltage disturbances standard (EN50160) [37], the voltage can be considered either a dip, normal operation or a short interruption, as shown in Figure 3.15 .

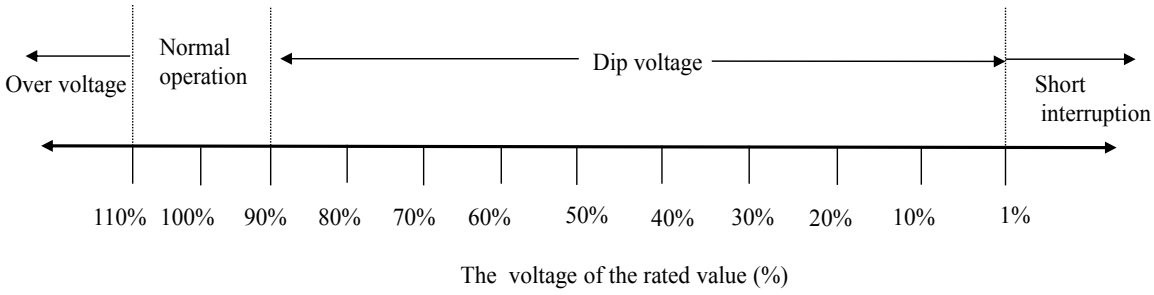

Figure 3.15 Voltage categories according to EN50160

Furthermore, the peak or depth voltage drop during a fault period can be defined as the measured point at the deepest point of voltage drop curve, as illustrated in Figure 3.16.

The main attention of this thesis is to improve the FRT by reducing the peak of the voltage drop during the fault period by increasing the reactive current. As mentioned earlier in the literature review, this can be done by applying various methods, some of which use crow bar protection [8, 12, 13], some of which apply modifications in the GSC control [15], and some of which modify the RSC controller [9, 17]. In this thesis, the RSC control has been modified to support the grid voltage.

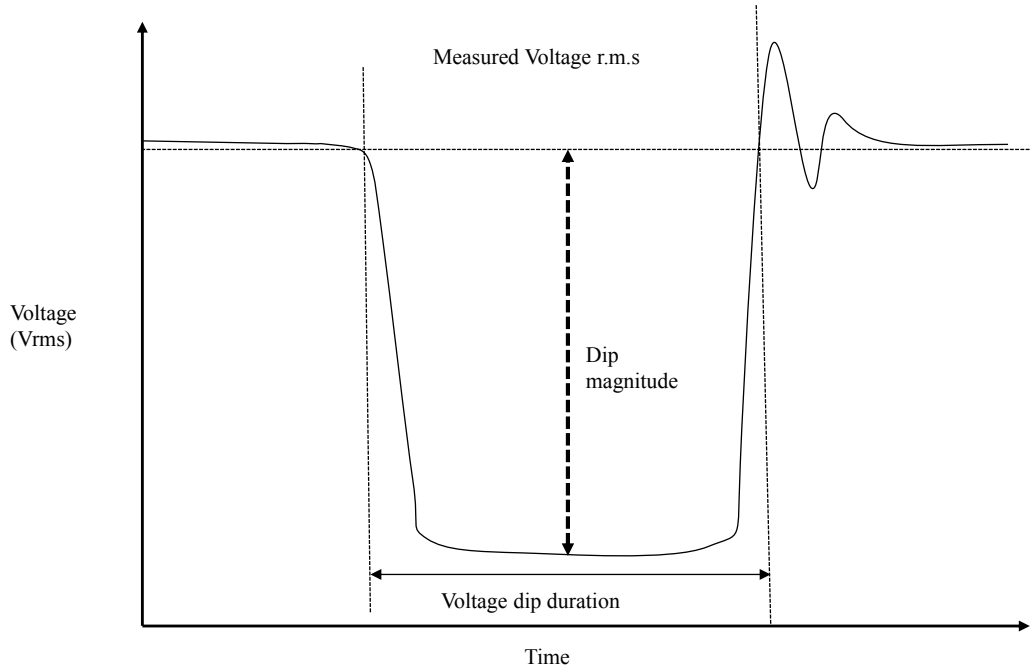

Figure 3.16 The depth voltage drop during a fault period [10]

3.5 MODIFICATION OF AN RSC CONTROLLER

In order to enhance FRT capability (which is the aim of the present thesis), the RSC control of DFIGs has been modified. The underlying concept for this technique is derived from three theories, as detailed below.

1. The performance of a DFIG during faults depends on the control of the DFIG [8]. As shown in Chapter 2, researchers are currently investigating RSC and GSC. The decoupling of controlling the active (P) and reactive power(Q) is achieved by applying the dq reference frame, and the RSC is the responsible for this controlling. Consequently, the main attention is focused on the RSC control.
2. The main idea for this work is derived from [9]. The authors modified the RSC so that the RSC supports the grid voltage with reactive power. They accomplished this

by modeling the RSC control as a combination of three different controllers: an electromagnetic torque controller, a current controller, and a voltage or reactive power controller, as shown in Figure 3.17.

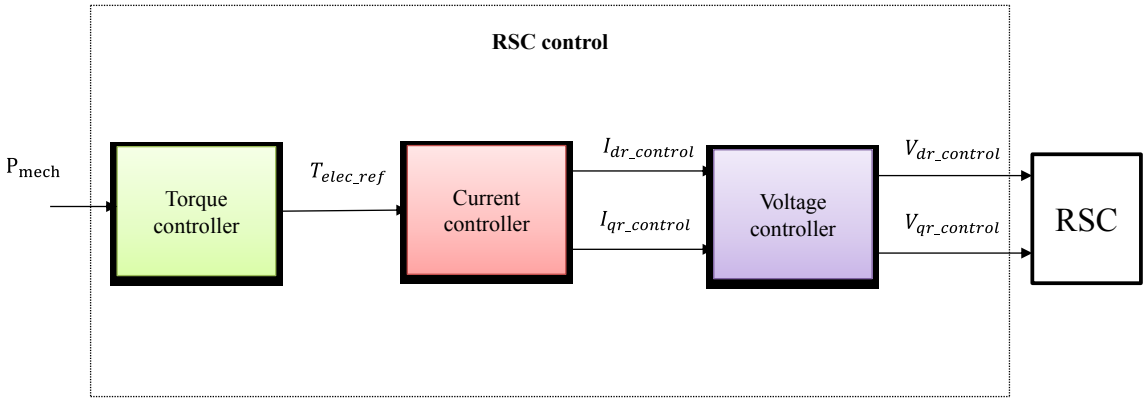

Figure 3.17 Three controllers are represented in the RSC controller [9]

The methodology of the electromagnetic torque controller, as Figure 3.18 shows, is to track the mechanical power (P_{mech}) of the turbine with respect to the turbine speed (w_{tr}). This can be done by using the drive train, as explained in section 3.3.2. This speed is then compared to the speed of the generator's rotor (w_{g_elc}) through the PI controller, after which the reference torque(T_{elec_ref})is determined, which is considered one of the inputs of the current controller to determine the reference rotor current in the frame d (I_{dr_ref}). As mentioned earlier, during grid fault, a high speed of the generator's rotor occurs. Consequently, based on generator speed, the I_{dr_ref} will be changed to support the grid voltage.

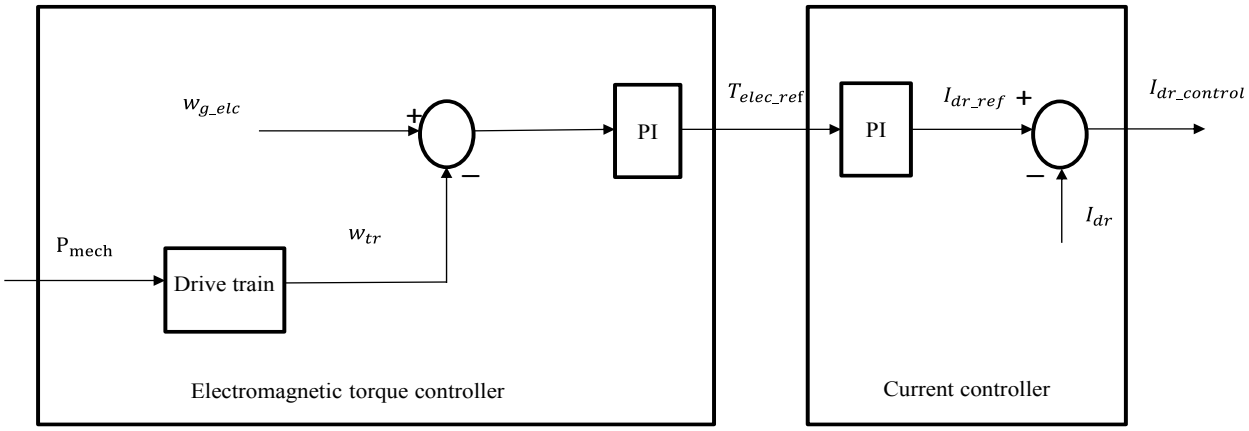

Figure 3.18 The electromagnetic torque and current controller

3. The drop voltage during the grid faults is a function of a fault current [10]

According to the three aspects listed above, instead of using an electromagnetic torque controller to determine the reference rotor current (I_{dr_ref})based on the generator's rotor speed (w_{g_elc}), this thesis proposes that a new external circuit controller be applied to set the reference of the current controller, as shown in Figure 3.19 .

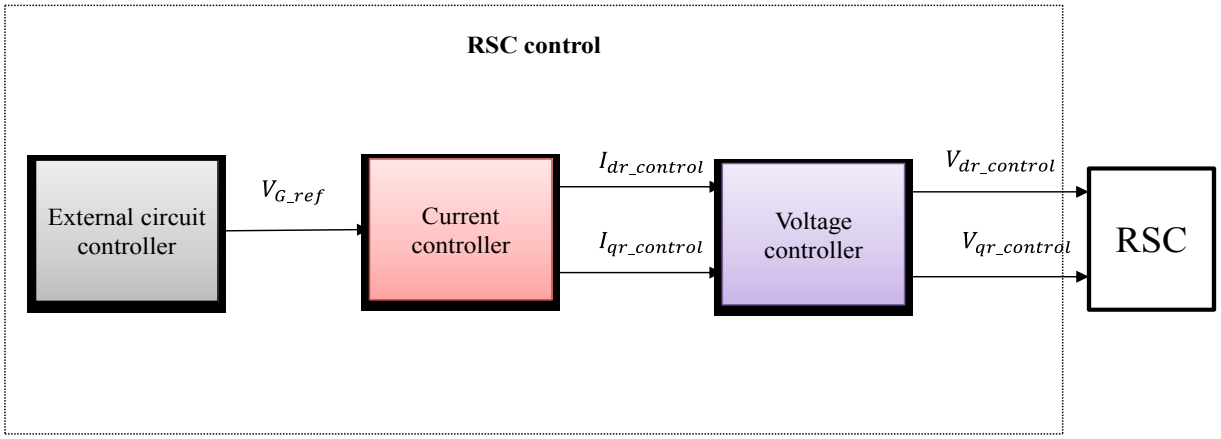

Figure 3.19 The new proposed RSC controller

3.5.1 The New Proposed External Circuit

The main aim of this circuit is to determine the reference voltage of DFIG V_{G_ref} which will be fed into the current controller to determine the I_{dr_ref} during steady state as well as during grid fault, as follows:

- During normal operation, the V_{G_ref} is calculated by measuring the voltage at the DFIG terminal (V_{G_mesu}) and comparing it with the voltage at the point of common coupling (V_{PCC}) through a PI controller.
- During grid fault, unlike in [9], the I_{dr_ref} was adjusted to improve the FRT capability of DFIG by T_{elec_ref} relatively to the speed of the speed of the generator's rotor. In this thesis, and according to the third theory, the $I_{dr_ref}$was adjusted by the V_{G_ref} comparatively to the fault current $i(t)$, following the DFIG. Therefore, a change in the reference voltage (ΔV_{ref}) based on the $i(t)$ will be proposed and applied. Thus, the ΔV_{ref} can be expressed by the fault current$i(t)$ and a factor(γ). This factor is defined here as an impedance-type factor related to the change in the reference voltage to the fault current. The ΔV_{ref} is described by the following equation (Ohm's Law):

$$\Delta V_{ref} = \gamma . i(t) \qquad (3\text{-}19)$$

where:

γ : the impedance-type factor

$i(t)$: the fault current

To accomplish this, a logic operator, switch and PI controller are implemented, so that the ΔV_{ref} is only applied if the voltage V_{pcc} dips under a minimum value. Figure 3.20 illustrates two cases of an external circuit, showing that the switch acts as a sensor that, only at specific conditions, allows the DFIG to support additional voltage relative to the fault current. Accordingly, the ΔV_{ref} will depend on the type and location of the fault.

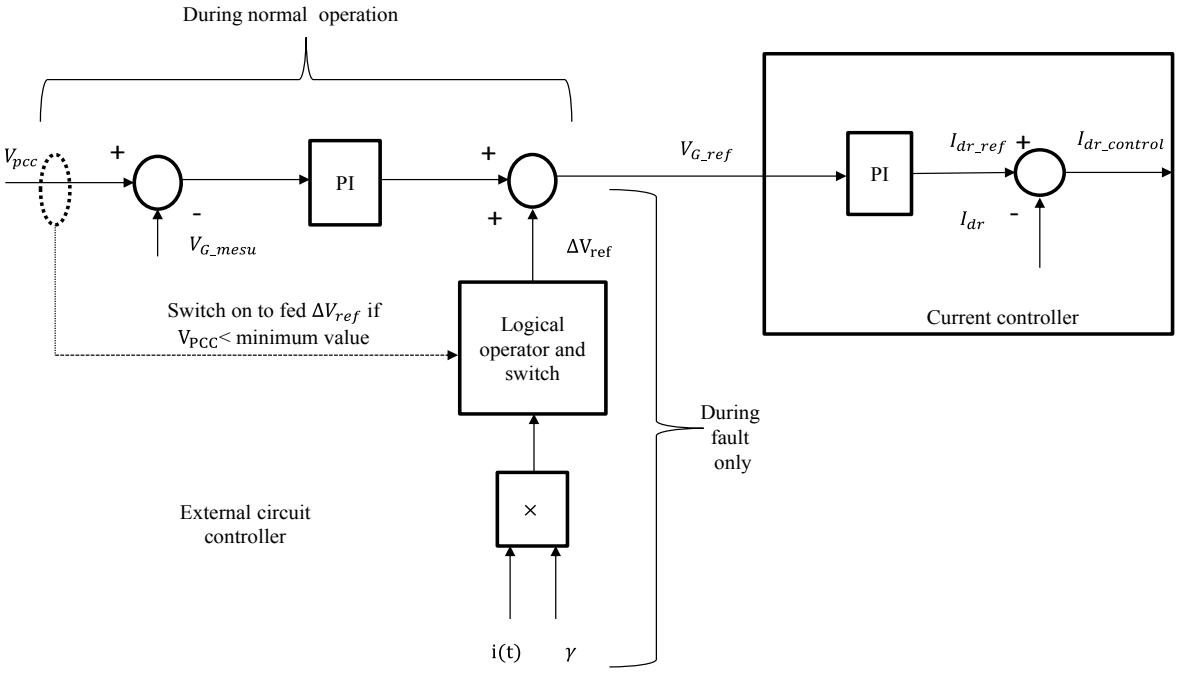

Figure 3.20 The proposed external circuit and current controller

For smooth reactive power control, a flexible AC transmission system (FACTS) can be the right option. Different types of FACTS can be used, such as a static synchronous compensator (STATCOM) depending on the desired options when a reactive current supply is required during grid faults [11]. The STATCOM provides reactive power at V_{pcc} and supports the grid voltage during voltages drop. Consequently, in this work, the FRT capability of DFIG is studied by utilizing STATCOM controllers.

3.6 THE STATCOM CONTROLLER.

The models of STATCOM controllers used in this thesis come from the MATLAB/SIMULINK library [38]. This controller consists of a current controller and a voltage controller. Additionally, the STATCOM controller is modeled in the dq reference frame, as shown in Figure 3.21.

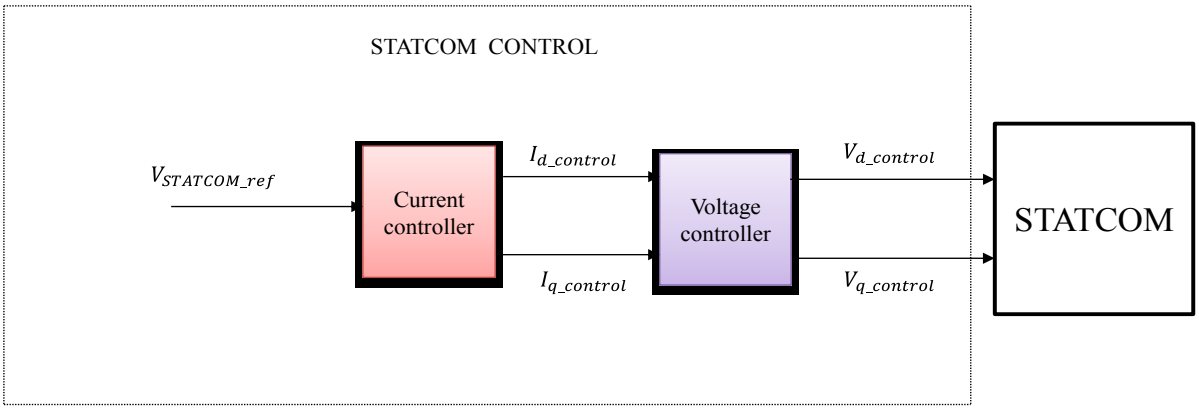

Figure 3.21 The STATCOM controller

As can be observed from Figure 3.21, the STATCOM controller is similar to the RSC controller, differing only in how it defines the reference of the STATCOM controller ($V_{STATCOM\_ref}$), as will be discussed later. The STATCOM located in the MATLAB/SIMULINK library has $V_{STATCOM\_ref}$ as a feature, generated either by the STATCOM itself or by an external value. Consequently, we exploited this advantage and applied the proposed external circuit in a way similar to the RSC control to the STATCOM control. In other words, we took into consideration that the $V_{STATCOM\_ref}$ is computed by measuring the STATCOM voltage ($V_{STATCOM\_mesu}$) and compared it with

the voltage at the point of common coupling (V_{PCC}), after which we injected the error through a PI controller, as shown in Figure 3.22.

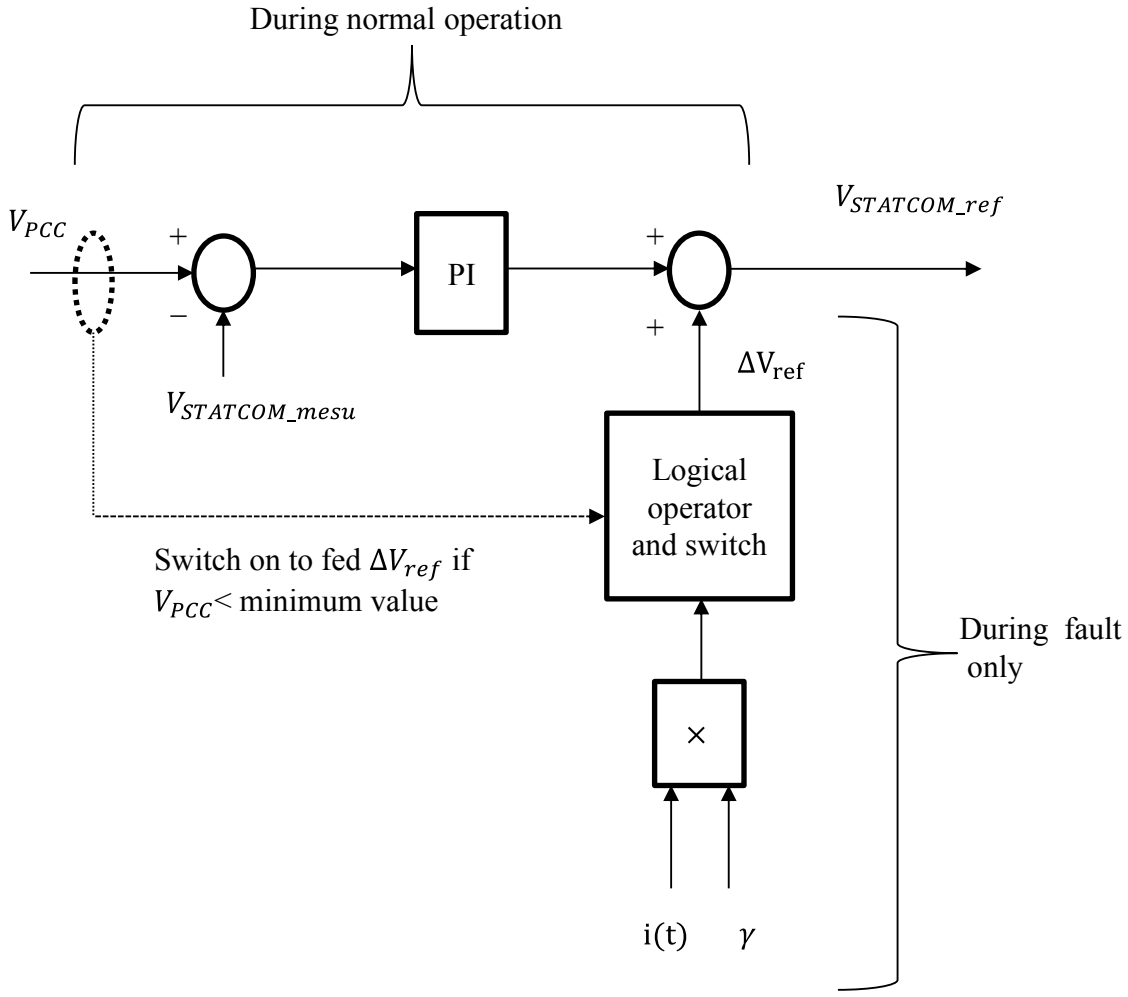

Figure 3.22 The proposed external circuit applied to the STATCOM controller

Consequently, by incorporating the two external circuits in Figure 3.20 and Figure 3.22 into one circuit, the new proposed external circuit was able to determine the V_{G_ref} and $V_{STATCOM\_ref}$ of the RSC controller and STATCOM controller, respectively, as illustrated in Figure 3.23.

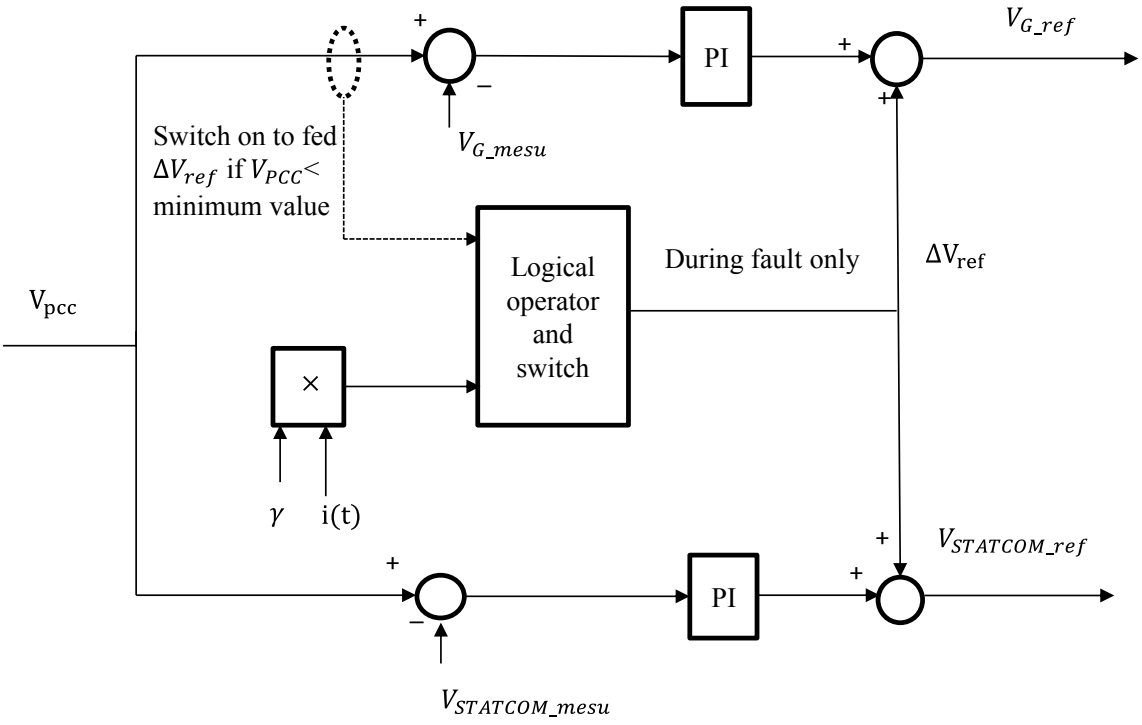

Figure 3.23 The proposed external circuit applied to the RSC and STATCOM controllers

Finally, this combined circuit was applied to the DFIG through the RSC controller and the STATCOM controller to achieve the flowchart, as shown in Figure 3.24. From this figure, the V_{ref_G} and $V_{ref_STATCOM}$can be determined by the external circuit, which is considered the first stage. The second stage is the current controller and voltage controller for both the RSC and STATCOM controllers. Figure 3.24 illustrates the methodology to achieve the aim of this thesis, which is improving the FRT capability of DFIG-based wind turbines.

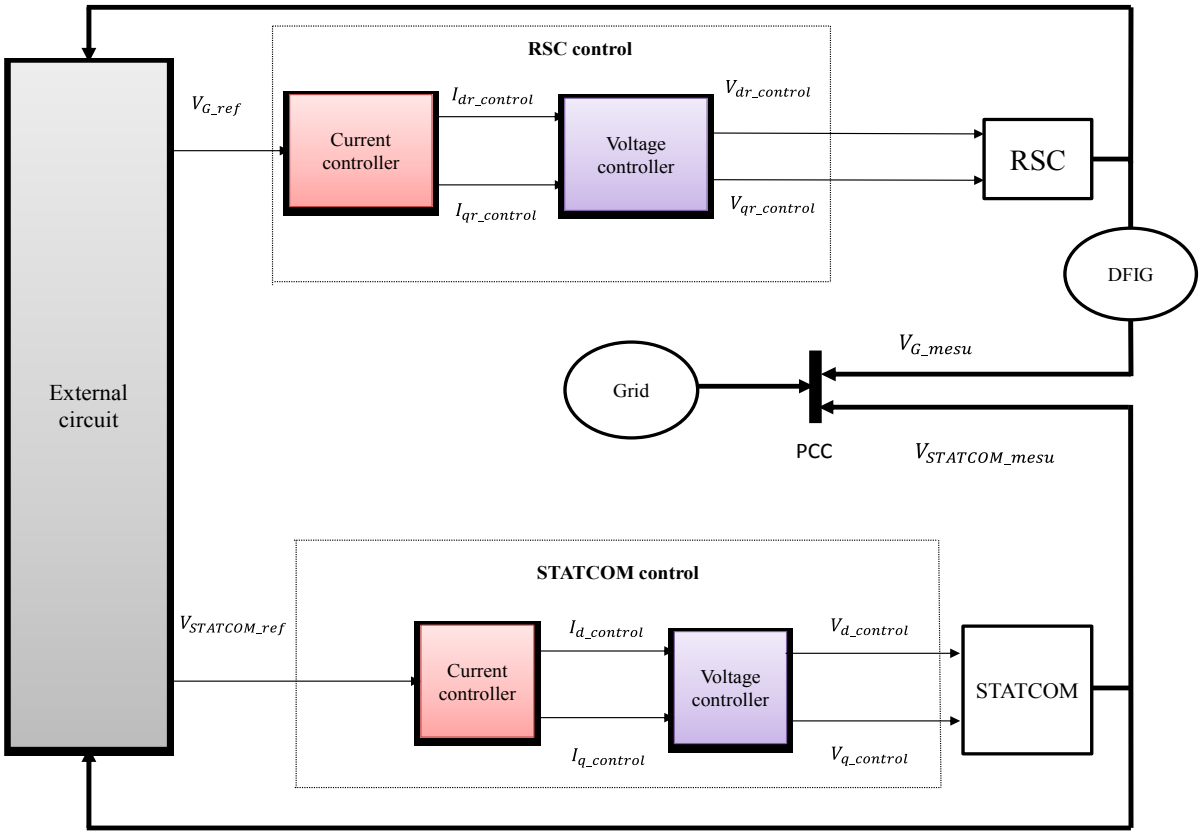

Figure 3.24 Voltage support at the point of common coupling by the DFIG and STATCOM

3.7 SUMMARY

In this chapter, a brief introduction to wind turbine-based DFIGs was introduced. An overview of wind turbine modeling was also provided, including the modelling of aerodynamic and the mechanical components. As well, this chapter covered examples showing the characteristics of a specific wind turbine, detailed the basic concept of DFIG and the purpose for using dq as a reference frame, and demonstrated the dynamic fifth order model of DFIG. Additionally, a brief introduction surrounding the behaviour and mode of DFIG during grid disturbances was discussed.

The main objective of this chapter was to present the external circuit as the methodology used in this thesis. Hence, the modification of the RCC controller was proposed and demonstrated, with the aim of improving the FRT capability of DFIG during faults. All issues related to enhancing the FRT capability of a DFIG coupled to a wind turbine during faults in next chapter are solved using the novel technique presented in this chapter.

CHAPTER 4 RESULTS AND DISCUSSION

4.1 INTRODUCTION

In Chapter 3, the improvement of the FRT capability of DFIGs during faults by using the external circuit method was introduced. In this chapter, the method will be implemented in MATLAB/Simulink environment on a Lenovo laptop processor Intel core 2Duo with 2.00 GHz and 4.00 GB RAM, using a block in the MATLAB/Simulink library [39], after which the results will be presented and discussed. The proposed method has been applied to reduce the peak of the voltage drop during a fault period. In this chapter, the results are presented to demonstrate the effectiveness of the method during faults, as follows:

1. In case one, the effectiveness of the method is tested at point B during a fault, as shown in Figure 4.1.
2. In case two, the effectiveness of the method is tested at PCC during a fault.
3. In case three, this method is compared to other methods to evaluate its efficiency.

The results obtained are compared with results obtained without using the proposed method, showing the method's effectiveness in the depth point of the voltage drop.

4.2 DESCRIPTION OF THE SYSTEM

A one-line diagram of the system is shown in Figure 4.1. As we can see, a wind farm of 9MW is connected to a 50Km distribution system. The distribution system is represented by a 25KV.60Hz, translating power to a grid represented by 120 KV. A step-down transformer 1 25KV/575V and transformer 2 120KV/ 25KV are applied. There are

five bus bars (B1, B2, B3, B4 and PCC) with voltages 575 V, 25KV, 25KV,120KV and 120 KV, respectively. As well, load and plant are connected to B1 and B3, respectively.

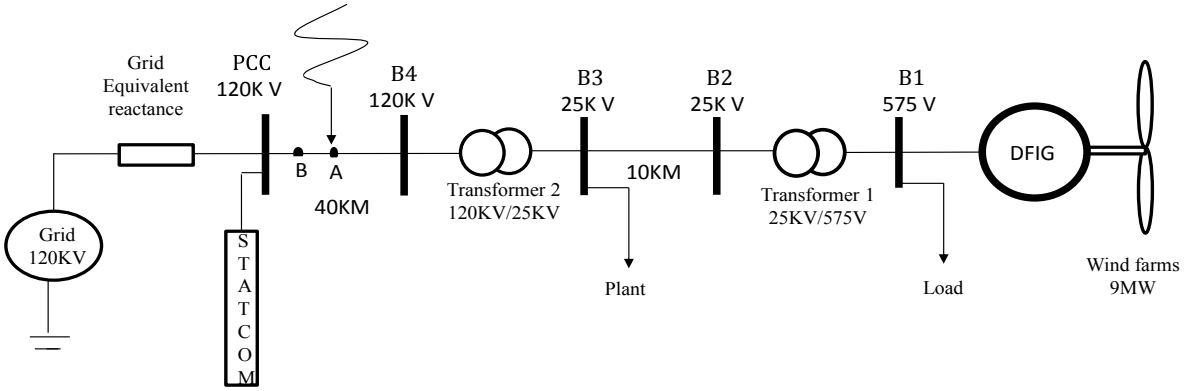

Figure 4.1 The system's one-line diagram

A wind turbine using the DFIG consisting of a stator is connected directly to the grid. In contrast, the rotor is connected to the grid via an AC/DC/AC IGBT-based pulse width modulation (PWM) converter, as shown in Figure 4.2.

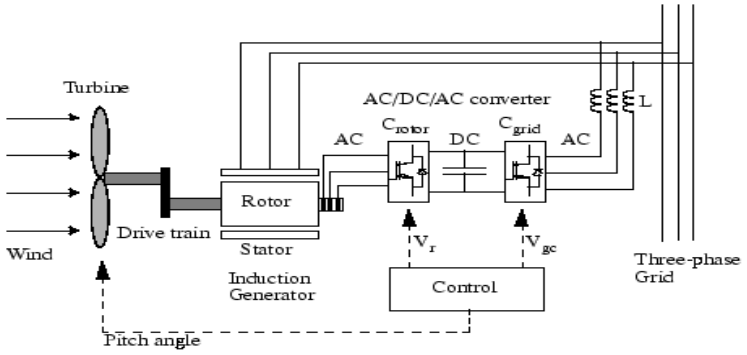

Figure 4.2 Wind turbines with doubly-fed induction generator [40]

The DFIG and wind turbine parameters are given in Appendix B. It should be mentioned that these data are similar to the small power transmission system model developed by mathworks in the Simpowersyst MATLAB/Simulink library [39]. In this thesis, there is a slight modification of the RSC controller, as mentioned in Chapter 3. Before studying the effect of the proposed method, more details about the other two components of the RSC controller are given below.

From Figure 4.3, it can be concluded that the objective of the external circuit is to generate the V_{G-ref}. This reference is injected to the current control through a PI controller (V-regulator) to define the reference rotor current in frame (d) (I_{dr_ref}). The reference rotor current in frame (q)(I_{qr_ref}) can be determined by controlling the active power. By comparing these reference currents with the actual rotor currents (I_{dqr}), the references of the voltage or reactive power control are achieved ($I_{dqr\_control}$). Furthermore, by injecting these values into the voltage controller through a PI controller (I-regulator), the reference rotor voltages are determined (V_{dqr_ref}), and by comparing these reference voltages with the actual rotor voltages (V_{dqr}), the outputs of the RSC controller are achieved ($V_{dqr\_control}$).

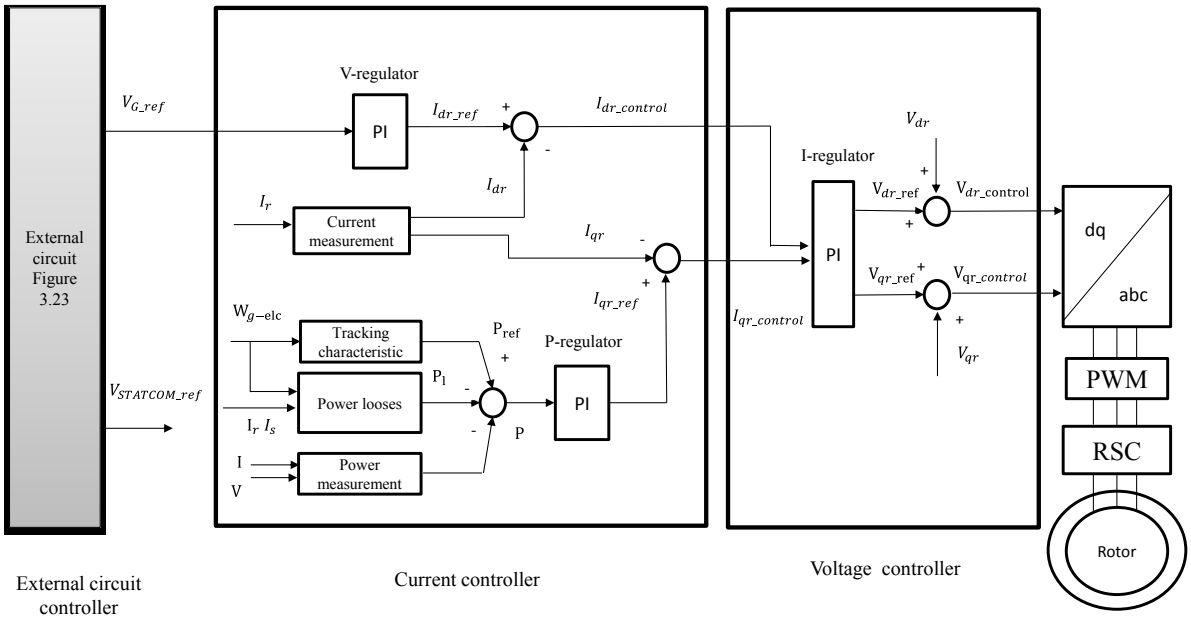

Figure 4.3 The three components of the RSC controller

Immediately, transforming the $V_{dqr\_control}$ from dq reference frame to abc frame and then feeding them to a 3-phase PWM and subsequently to IGBTs with universal bridge. V and I presented in the Figure 4.3 are represented the voltage and current at B1 respectively. The data of the external, current and voltage controllers are given in Appendix B.

The wind turbine-based DFIG model and the external circuit in MATLAB/Simulink are shown in Figure 4.4 and Figure 4.5, respectively. It should be noted that there is no modification regarding the GSC controller, which already existed in [40]. As mentioned in section 3.3.5, the duty of GSC is to keep the voltage of the DC-link constant.

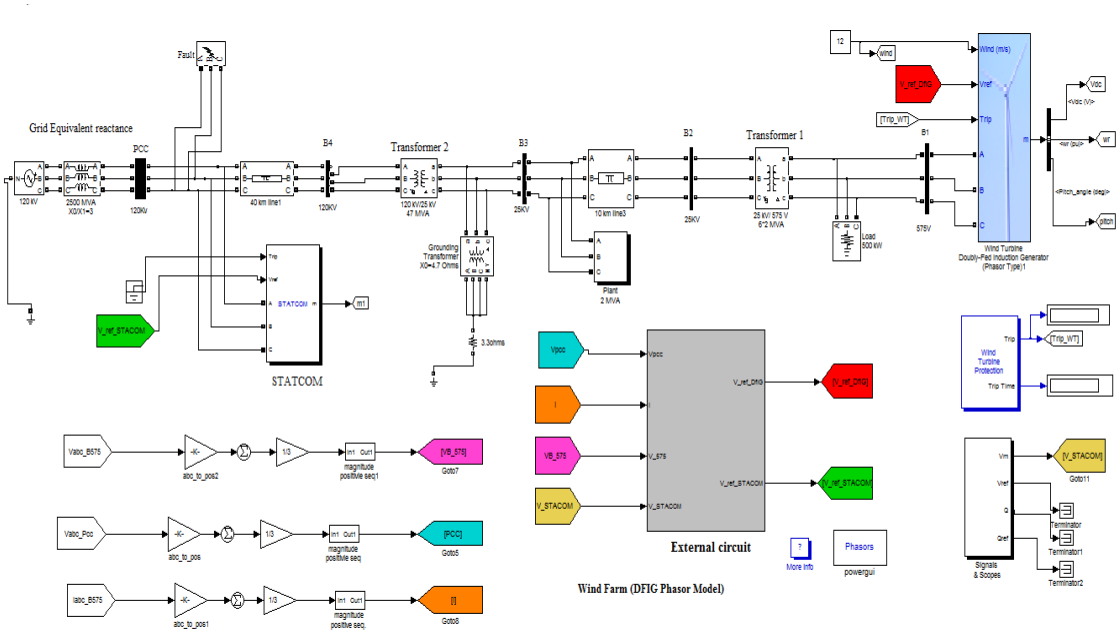

Figure 4.4 The MATLAB/Simulink model with the external circuit

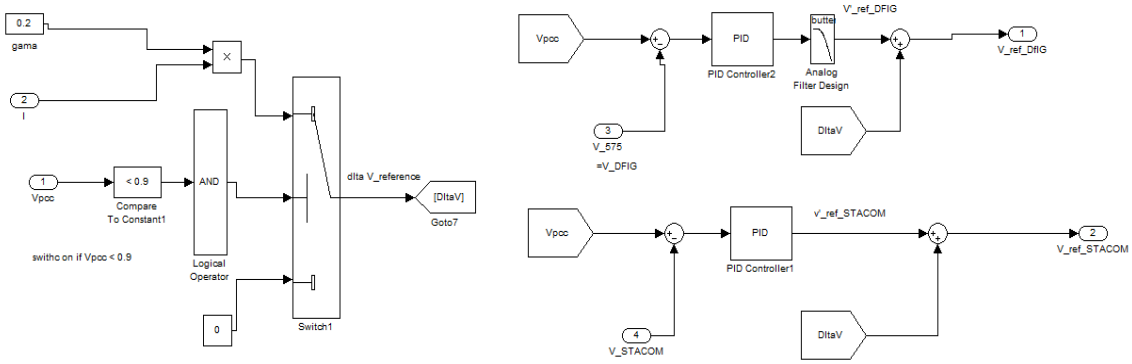

Figure 4.5 The external circuit

4.3 CASE STUDIES

In this section, the dynamic interaction and performance of DFIG-based wind turbines with power transmission systems during faults are illustrated and discussed. Three cases will be simulated and studied. The objective of the first case is to test the proposed method to improve the FRT capability of DFIGs at point B by considering a short-circuit grid fault at the end of a 40Km transmission line at point A (close to PCC) and study the voltage support during a fault. In the second case, the effect of the method at the PCC during a fault will be studied and the results obtained when using the proposed external circuit will be compared with those obtained when the proposed method is deactivated. In the third case, the present method will be compared with other methods mentioned in the literature review. To study faults, the DFIG and STATCOM models are set at a phasor simulation type to allow transient stability studies with a long simulation time [39].

A short-circuit grid fault with fault resistance($R_f = 1 \times 10^{-3}\Omega$) and ground resistance ($R_g = 1 \times 10^{-3}\Omega$) occurs at point A at t=5 seconds, with a clearance time of 150(ms). The wind speed is kept constant at 12(m/s). The proposed external circuit in Figure 3.23 is connected to the RSC of the DFIG and to the control circuit of STATCOM. It feeds the ΔV_{ref} whenever V_{pcc} dips under a minimum value to support the system voltage. According to Figure 3.15, this minimum value can be equal to 0.9(pu). Through trial and error experiments, the impedance-type factor (γ) is rated at 0.2(pu), to give an optimum value of ΔV_{ref}. As a result, there is better voltage support to the grid, with $i(t)$ being the fault current flowing toward the DFIG, measured at B1. It shoud be mentioned that, the results are within practical guidelines for circuit breaker allowable time limits.

4.3.1 Case study 1: Voltage Support at Point B During Grid Faults

As is generally known, voltage dips can be divided into two classifications: balanced fault and unbalanced fault. Therefore, one-phase, two-phase, and three-phase grid faults are applied at point A. Simulated results of these faults are presented in Figure 4.6, Figure 4.8 and Figure 4.10. In all fault test cases, comparisons of obtained results without using the external circuit and with the proposed circuit results show that the proposed circuit method achieves significantly better results regarding voltage support during grid fault. It should be noted here that an external circuit case is simulated by connecting the external circuit, and the obtained results show the effectiveness of the ΔV_{ref} and STATCOM.

The response to ΔV_{ref}, where the voltage at point B dips under 0.9(pu), is illustrated in Figure 4.7, Figure 4.9 and Figure 4.11. From all of these figures, a variation of ΔV_{ref} between the different types of faults can be discerned. This is because the fault, $i(t)$, and consequently the ΔV_{ref} at the three-phase grid fault, are considered high. Hence, the external proposed method has been successfully used to support voltage during grid fault and improve the FRT, especially when three-phase faults occur, as Table **4.1** Comparison between the voltage support of different types of faultsTable 4.1, Figure 4.12 and Figure 4.13 show. From this, it can be concluded that voltage support by the proposed external circuit is done relative to theΔV_{ref} and subsequently to $i(t)$, as explained in the methodology of this thesis.

Table 4.1 Comparison between the voltage support of different types of faults

	Voltage at point (B)		
	The average of voltages obtained are within prescribed standard limits (pu)		Voltage support (%)
	Without external circuit	With external circuit	
One-phase fault	0.7481	0.7533	0.52
Tow-phase fault	0.7438	0.7492	0.545
Three –phase fault	0.7428	0.7486	0.58

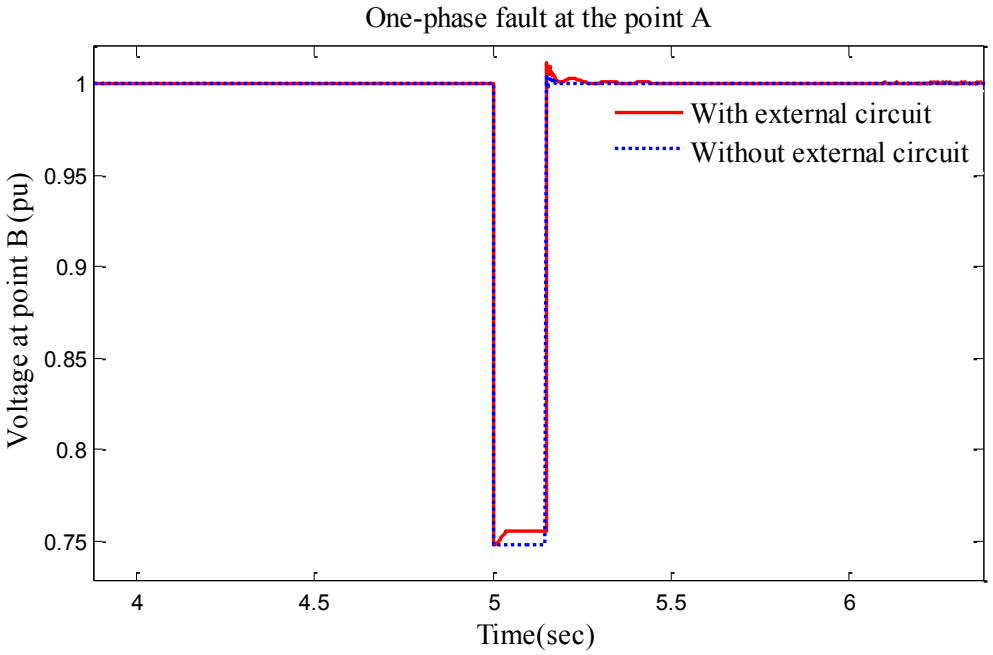

Figure 4.6 Positive sequence voltages at point B during a one-phase grid fault

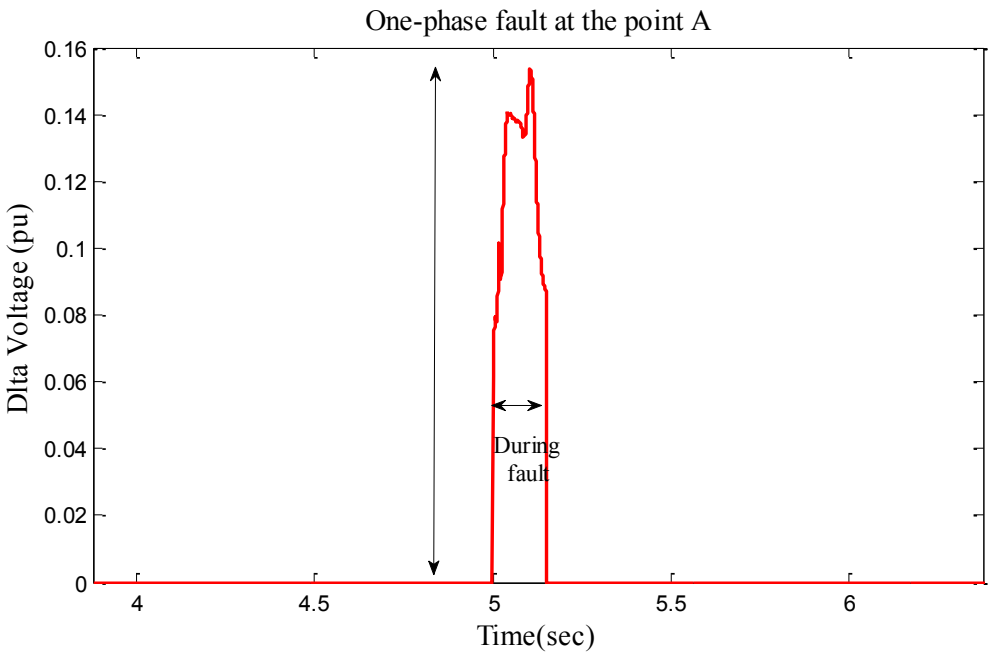

Figure 4.7 The response of ΔV_{ref} during one-phase grid fault

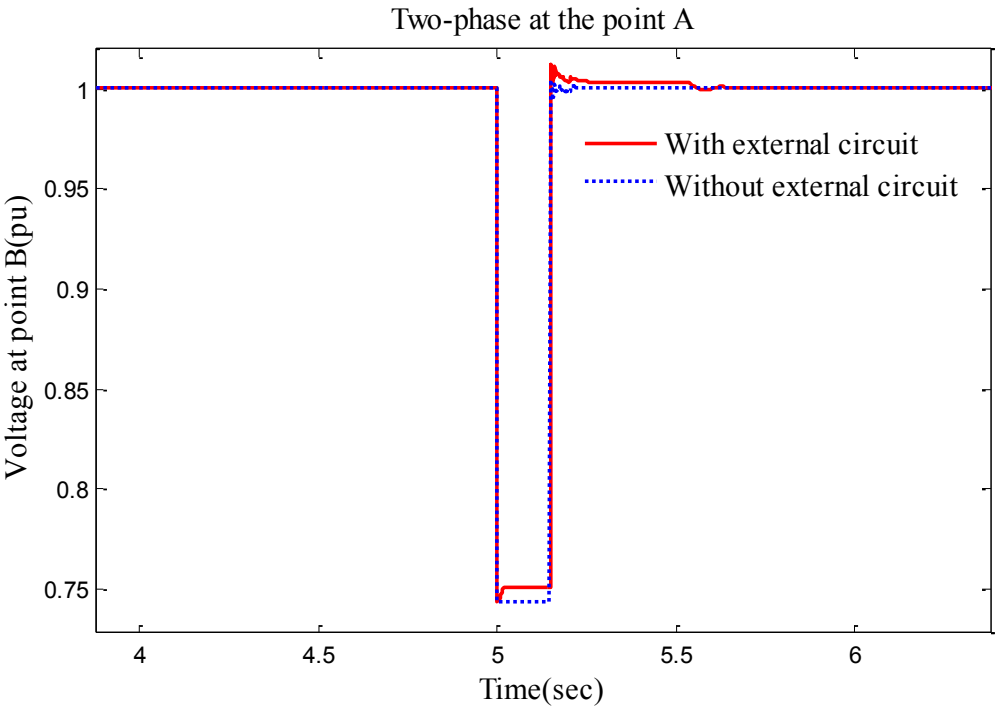

Figure 4.8 Positive sequence voltage at point B during a two-phase grid fault

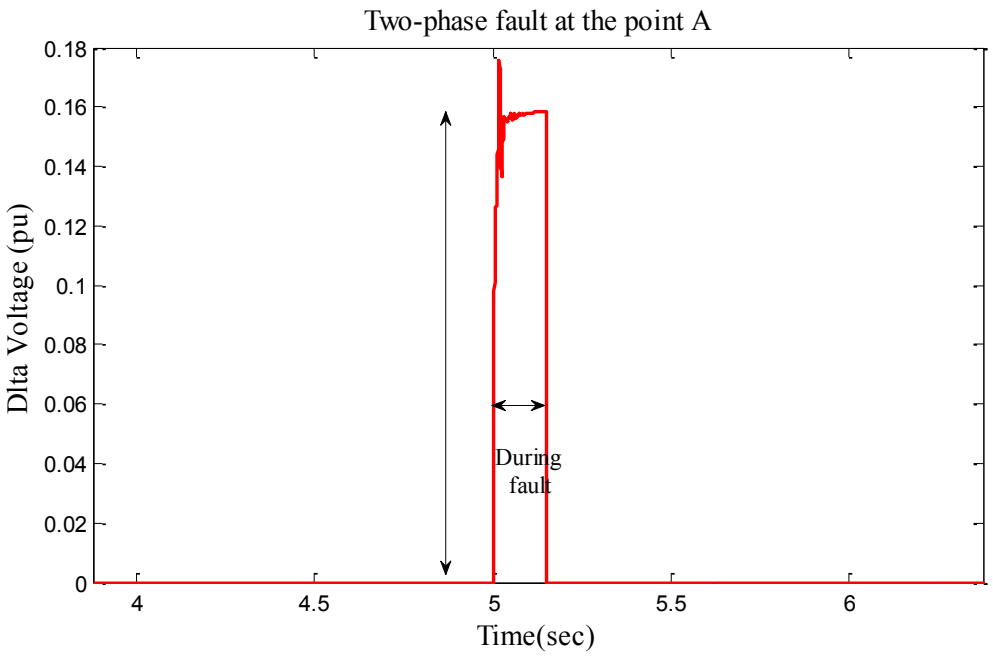

Figure 4.9 The response of ΔV_{ref} during two-phase grid fault

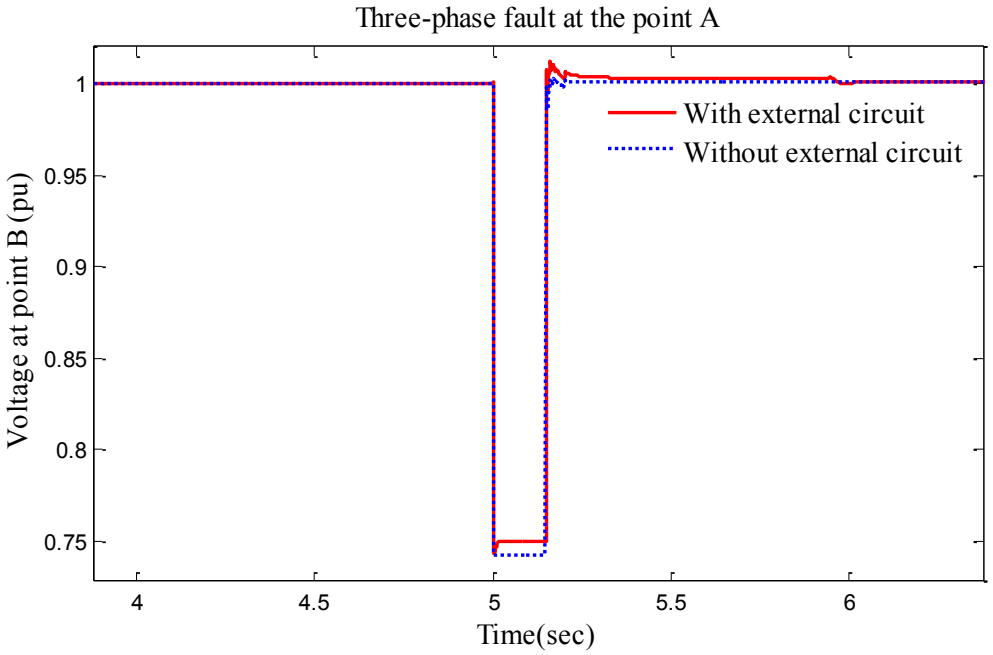

Figure 4.10 Positive sequence voltage at point B during a three-phase grid fault

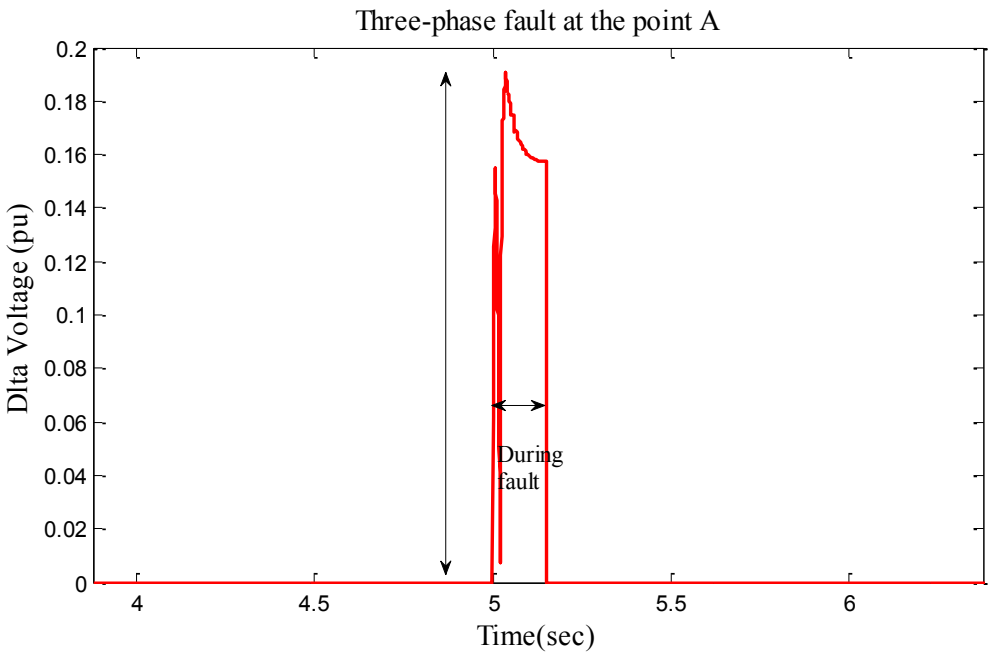

Figure 4.11 The response of ΔV_{ref} during a one-phase grid fault

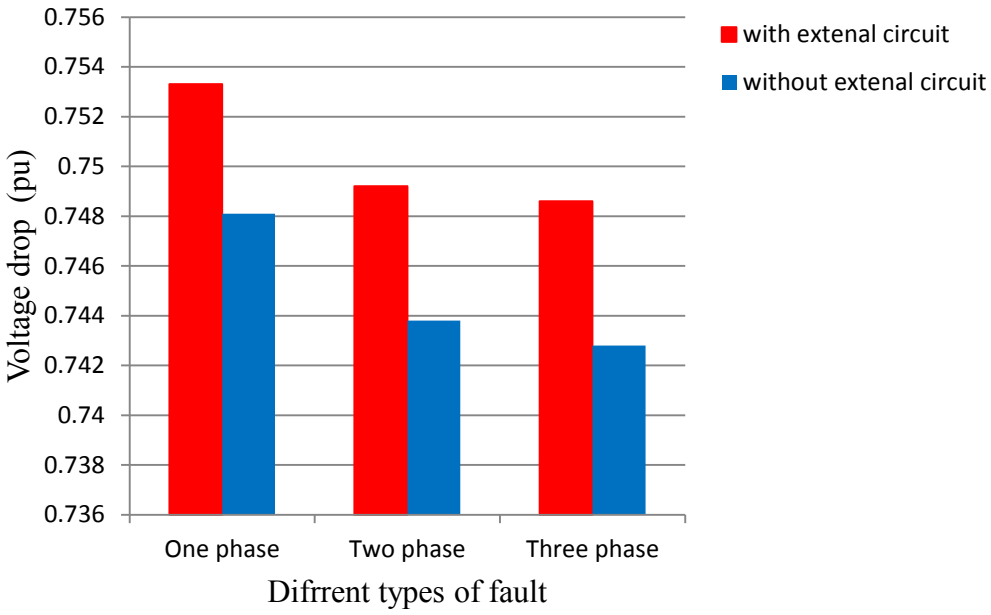

Figure 4.12 Comparison of the voltage drop between the three types of faults

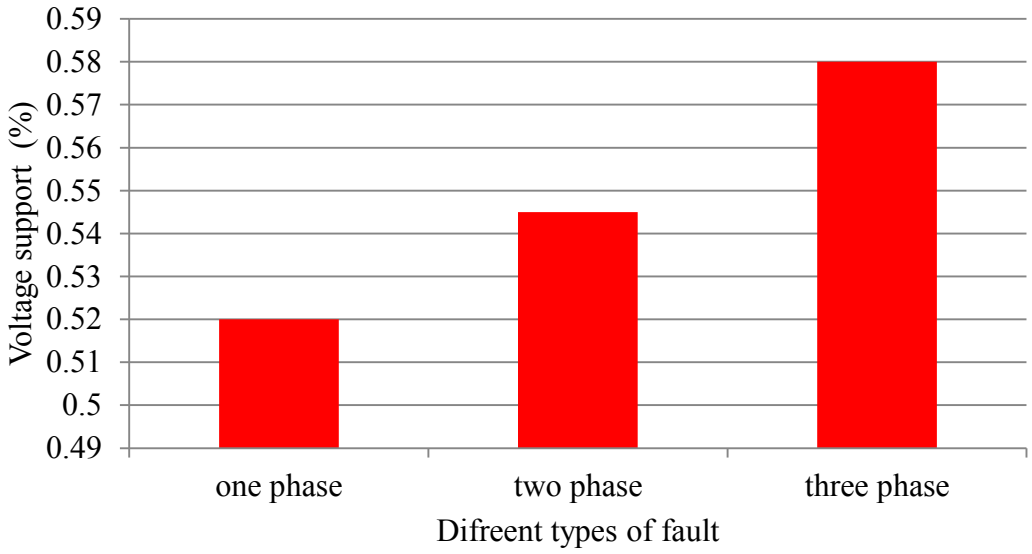

Figure 4.13 Comparison of the voltage support between three different types of faults when using the extenal circuit

4.3.2 Case study 2: Voltage Support at PCC During Grid Faults

In the present case, the external circuit is applied to enhance the FRT capability of DFIG and support voltage at PCC during grid faults. Figure 4.14, Figure 4.15 and Figure 4.16 show a comparison between voltage recovery with and without using the proposed method.

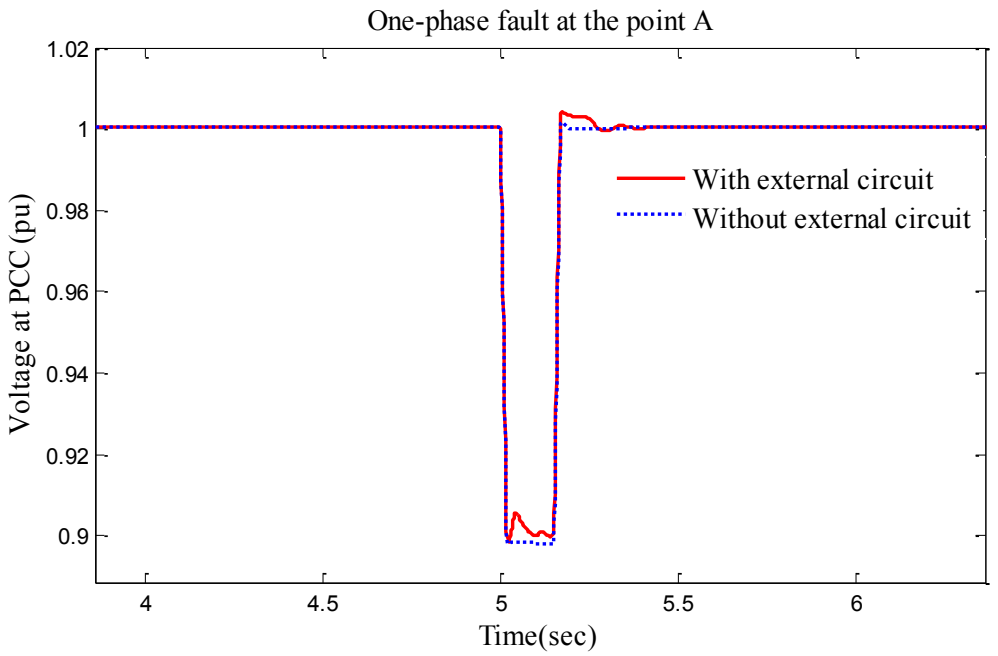

Figure 4.14 PCC voltage using the external circuit during a one-phase grid fault

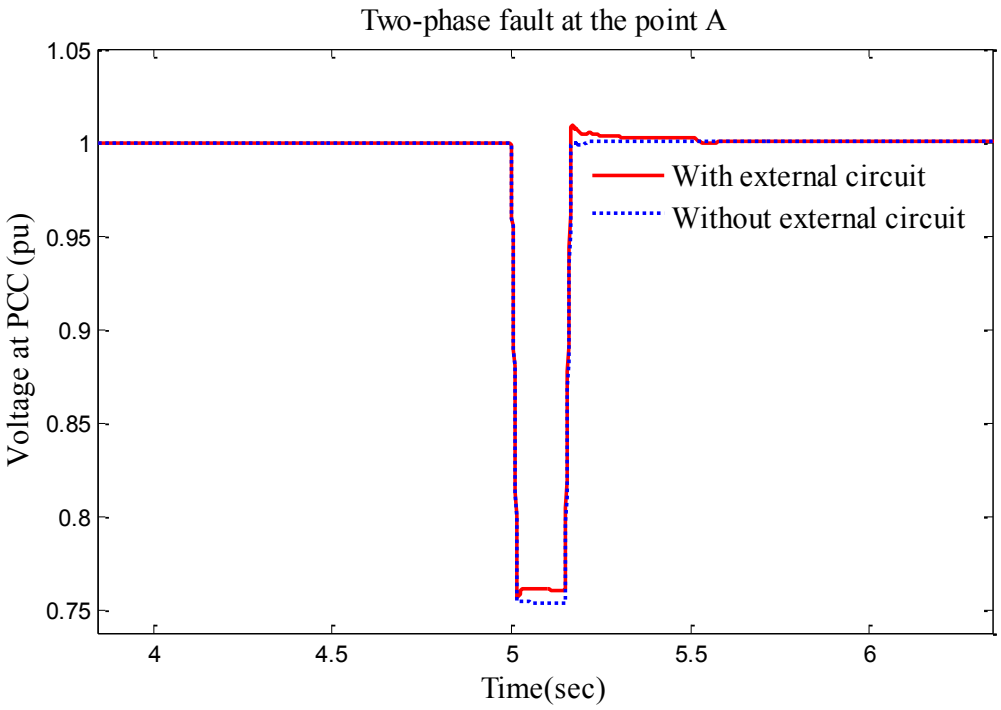

Figure 4.15 PCC voltage using the external circuit during a two-phase grid fault

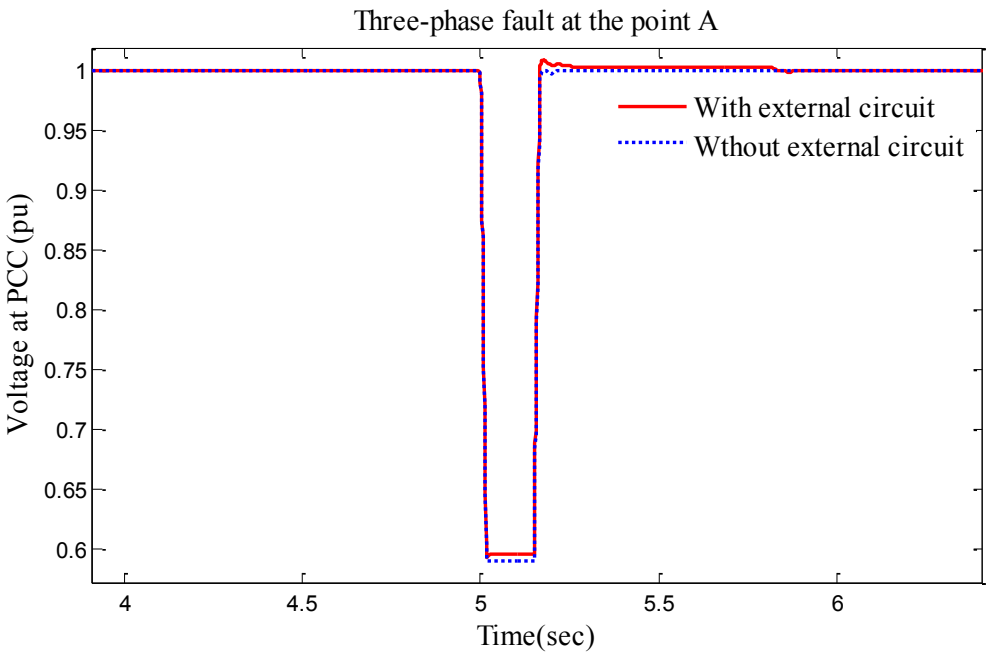

Figure 4.16 PCC voltage using the external circuit voltage support during a three-phase grid fault

Table 4.2 Comparison of voltage support during a fault with and without using the external circuit

	Voltage at PCC		
	The average of voltage obtained are within prescribed standard limits (pu)		Voltage support (%)
	Without external circuit	With external circuit	
One-phase fault	0.8983	0.9015	0.3176
Two-phase fault	0.7539	0.7579	0.405
Three-phase fault	0.59	0.5944	0.4417

The following conclusions can be drawn from the results presented in Table 4.2. The voltage support at the PCC is comparatively small; nevertheless, the results of the voltage drop clearly show that the proposed external circuit has achieved significantly good results in the FRT, especially when compared to results obtained without the external

circuit. Moreover, the voltage support results show that the three-phase fault case has the best voltage support compared to one- and two-phase faults due to the change of ΔV_{ref} according to $i(t)$. In the next subsection, the reactive power generated by the DFIG in a different mode will be simulated and discussed.

4.3.2.1 The Reactive Power Generated by DFIG During FRT

In the following, the response of the DFIG with the external circuit during FRT under three-phase grid faults is simulated and two different modes of DFIG (under-excited and over-excited) are considered.

Before and after a fault occurred, as shown in Figure 4.17, the DFIG in under-excited mode, which means, the DFIG will attempt to absorb the reactive power (see Figure 3.13) around 1.3MVAr limits. During a fault, a fault current flows from the grid into the DFIG. In this state, the DFIG will generate and supply reactive power by the RSC, this can be done by using the temporary overload capability of DFIG [11] in order to support grid voltage recovery. Likewise, when the DFIG is in over-excited mode (as illustrated in Figure 4.18) before and after the fault occurred, the DFIG (according to Figure 3.13) supply around 1.8MVAr reactive power to raise the grid voltage. In fault instance, same way of the above case ,the DFIG will generate and supply reactive power To sum up, for both modes of DFIG during a grid fault, the DFIG would fulfill the grid requirement and supply the system via reactive power.

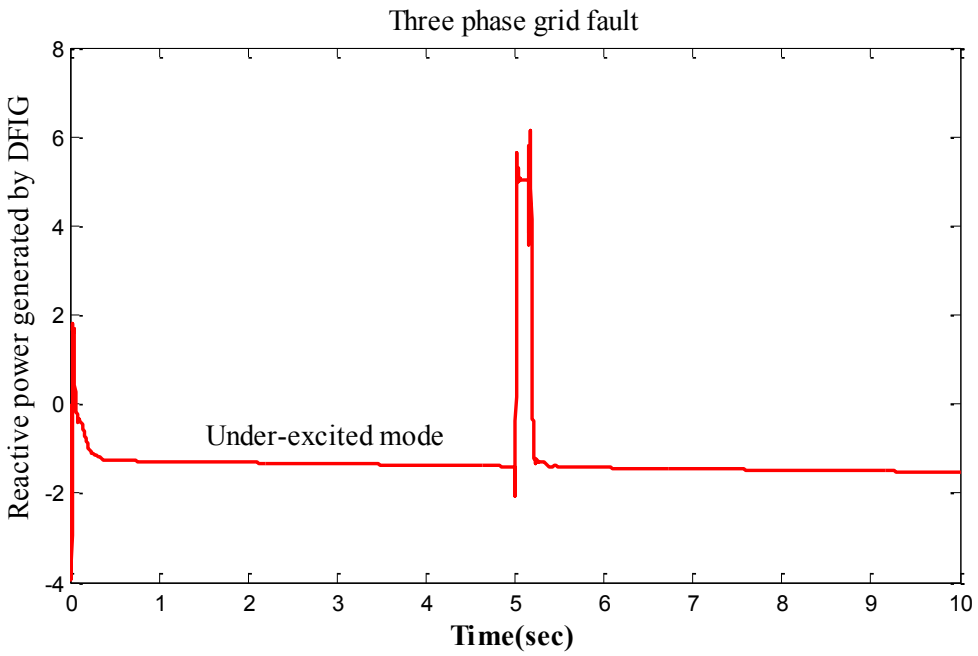

Figure 4.17 Reactive power generated by DFIG at under-excited mode and during FRT

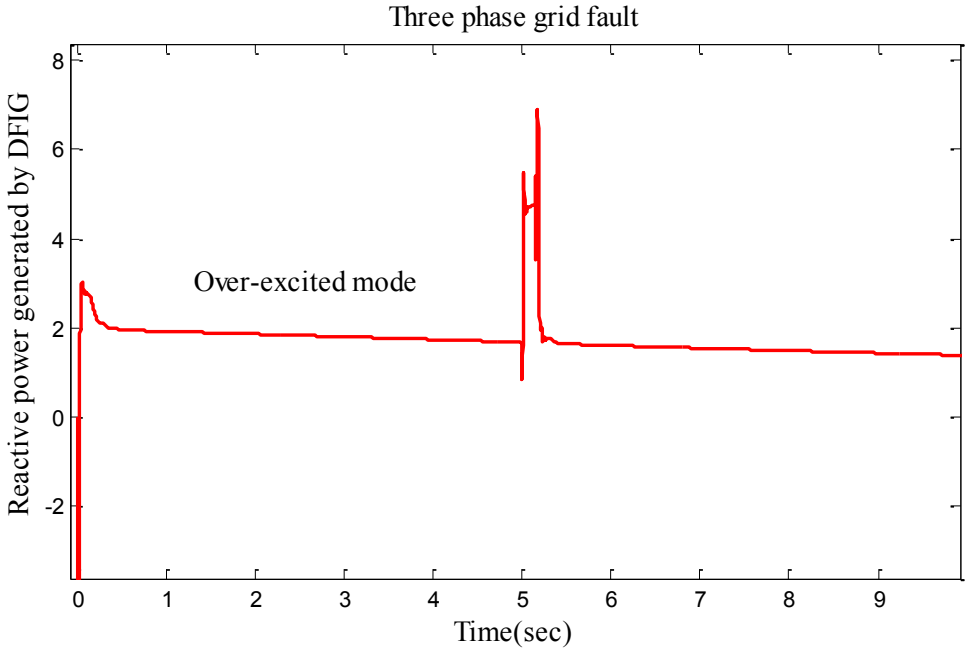

Figure 4.18 Reactive power generated by DFIG over-excited mode and during FRT

Figure 4.19 shows the reactive power supplied by both modes during FRT. As can be observed, the DFIG in under-excited mode supplies more reactive power than in-over excited mode, proving one of the characteristics of the DFIG stated in Chapter 3.

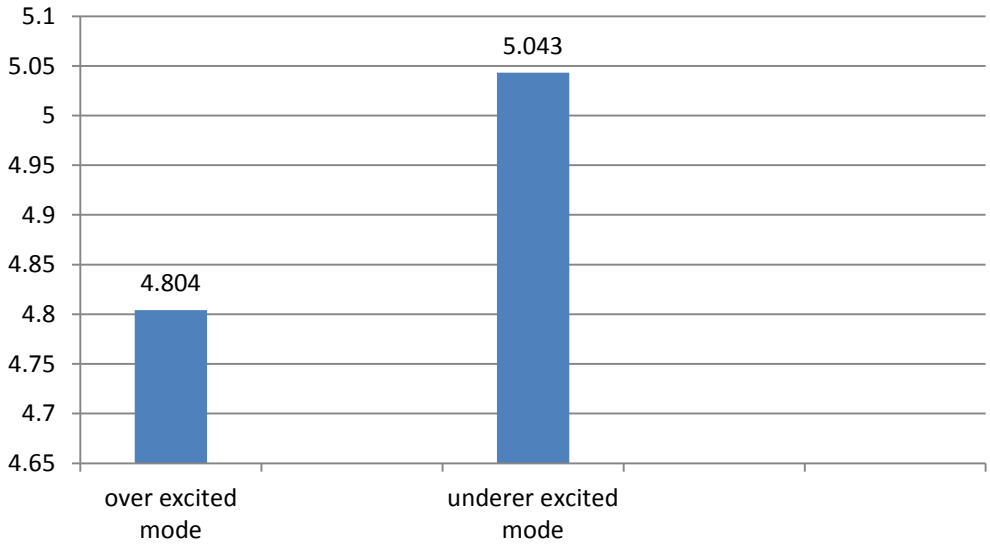

Figure 4.19 Average reactive power supplied during FRT for different modes of DFIG

As a final point in this subsection, comparisons will be simulated to check the effectiveness of the external circuit on reactive power supplied by the DFIG in unity mode. Two different scenarios are analysed – the first scenario is without the external circuit and second one is with the external circuit. Both scenarios are illustrated in Figure 4.20. As can be seen, the reactive power supplied in the second scenario is substantially higher than power supplied in the first. This result explains why the voltage dips in the second scenario are frequently smaller than in the first scenario.

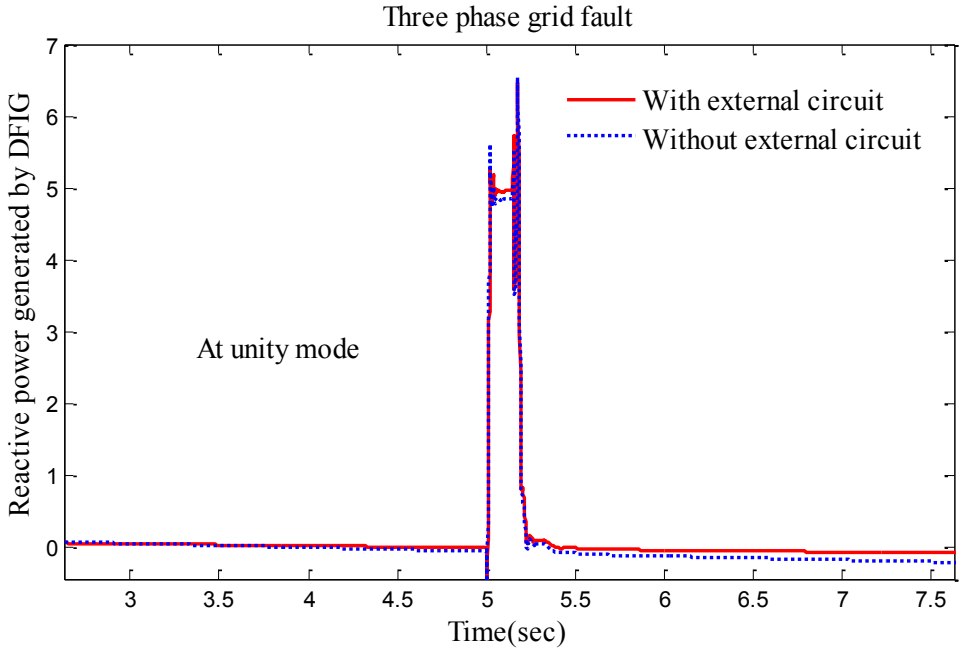

Figure 4.20 Reactive power generated by the DFIG at unity mode and during FRT

4.3.3 Case study 3: Evaluation of the Method

In order to test the effectiveness of the proposed external circuit during a grid fault, the proposed method will be compared to the crowbar protection method, after which the impact of ΔV_{ref} will be discussed. Subsequently, a comparison between current and novel methods, as listed in Chapter 2, is provided.

4.3.3.1 The Impact of Crowbar Activation During FRT

The crowbar impact was reported in detail in Chapter 2 and its disadvantages were summarized in Chapter 3. In this section, to demonstrate the undesirable effect of crowbar protection on voltage recovery during a fault, voltage support is simulated by activating crowbar during a one-phase grid fault at point A. Here, the activation of crowbar can be

occur in two situations: (1) when the rotor current increases and exceeds the maximum limit; and (2) when the DC-link voltage increases and overshoots the maximum limit [9]. In this thesis, the second situation is simulated. Basically, in a fault instant, the DFIG draws fault currents from the grid into the DC-link located in the converter. These currents reverse the diodes which are connected with IGBTs, causing a high voltage of the DC-link. As a result, the crowbar protection circuit will be switched on and activated [11].

To do this, in the protection system of the MATLAB/Simulink model in Figure 4.4, the DC-link voltage is set to maximum value so that, during grid fault, the DC-link voltage will exceed this maximum value. A simulation of the system is carried out in Figure 4.21, where it can be seen that the fault happens at 5(sec) with crowbar protection. Additionally, the figure shows the voltage at PCC before and after the fault, with a comparison between the proposed external circuit and the crowbar method.

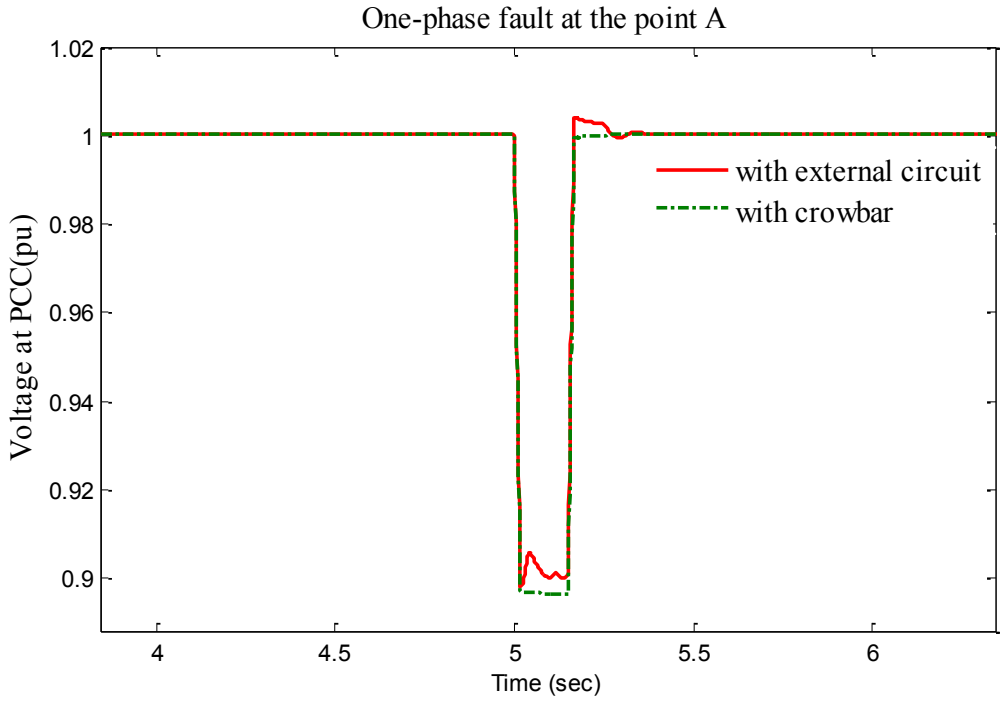

Figure 4.21 Voltage at PCC using different methods of FRT for improvement

Table 4.3 Comparison of PCC voltages between different cases of FRT to FRT with crowbar

	Voltage at PCC (pu)	
	Voltages obtained are within prescribed standard limits	
	With external circuit	With crowbar protection
One-phase fault	0.9057	0.8966

The following conclusions can be drawn from the results presented in Table 4.3. The voltage dip at PCC during a fault is around 0.8966(pu) when the crowbar circuit is activated. This can be considered the worst case scenario because the controllability of DFIG is lost and the DFIG would behave as a squirrel cage induction generator; however, with the proposed external circuit, the dip is around 0.9057(pu). Consequently, it can be concluded that the best FRT can be achieved without crowbar protection. Indeed, [11]

reported that the majority of modern wind turbines coupled to DFIG attempt to ride through the fault without activating the crowbar.

4.3.3.2 The Impact of the Delta Reference Voltage (ΔV_{ref})

In this subsection, the evaluation of the weight of ΔV_{ref} is presented. The simulations were first done without connecting the ΔV_{ref} of the external circuit to the STATCOM and RSC controllers. in other words, during FRT, the ΔV_{ref} was deactivated. Next, in comparing the results obtained from the above to the results obtained when using the entire circuit (including the ΔV_{ref}) it is clear that, during a grid fault, the lowest voltage dip of 0.78(pu) at 5.1(sec) occurs when the ΔV_{ref} is deactivated. On the other hand, the voltage dip improves dramatically – to about 0.79 (pu) – when the ΔV_{ref} is activated .as Figure 4.22 shows

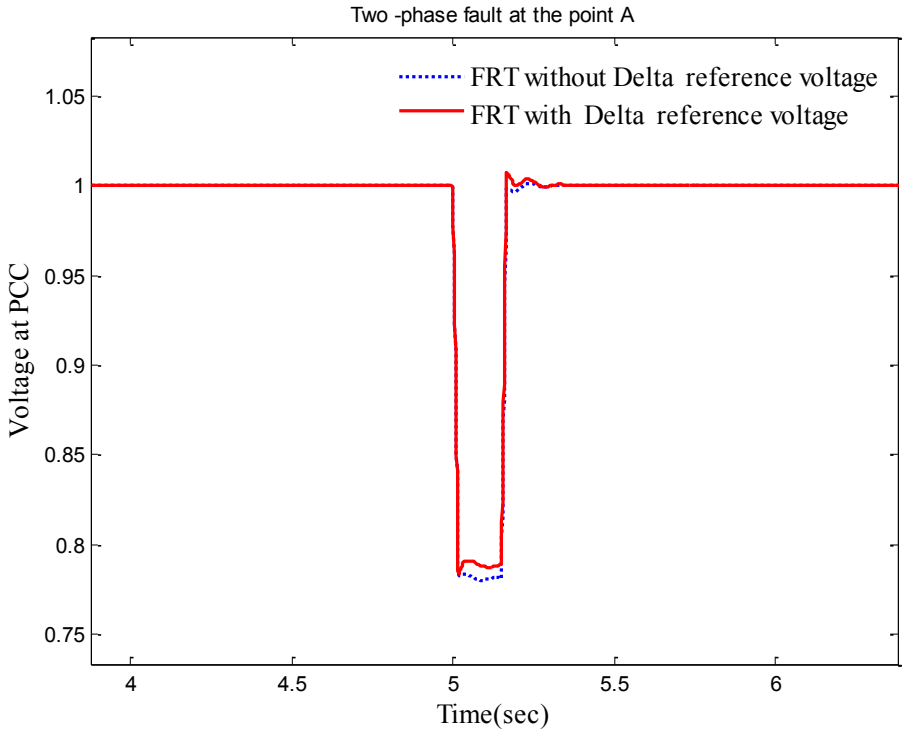

Figure 4.22 The effect of deactivating the ΔV_{ref}

4.3.3.3 Comparison Between the External Circuit Method and Various FRT Methods

In this subsection, the FRT obtained by the proposed method is compared with some other methods listed in the literature review [9]. The researchers also modified the RSC controller and used the STATCOM to study the FRT capability of DFIG at (B1). Therefore, the voltage at B1, which is called the DFIG terminal, will be simulated during a three-phase grid fault and two different cases are implemented. The first case is without the external circuit and the second case is with it, as shown in Figure 4.23.

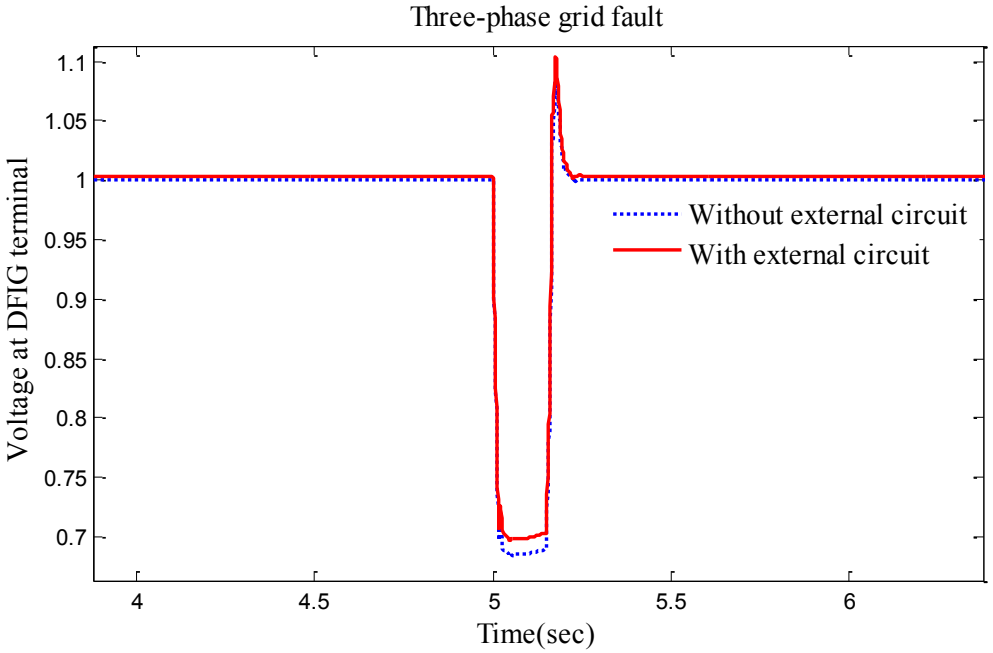

Figure 4.23 Voltage at a DFIG terminal during a three-phase grid fault

Before and after the fault, the voltage at the DFIG terminal in the second case is the higher compared to the first case. During the fault, the first case has the lowest voltage dip of 0.68 (pu) at 5.04 (sec). In contrast, the voltage dip improved significantly to 0.7 at 5.04(sec) in the second case.

In [9], two additional cases were analyzed. The first case featured no voltage support and the second case featured modified RSC control and STATCOM. During the fault, the first case showed a voltage dip of 0.53 (pu) at 5.03, while in the second there was no indication of the value of the voltage drop. To find the value, Graph Click software was utilized and revealed voltage drop to be around 0.55 (pu). A comparison of the two methods is illustrated in Table 4.4.

Table 4.4 Comparison of the voltage support obtained by the proposed method and the method in [9]

Method	Modification of RSC controller	Methodology of voltage support	Average voltages obtained are within prescribed standard limits (pu)		Voltage support during fault (%)	Reactive power source
1. [9]	Combined from electromagnetic torque, current, and voltage controllers	Relative to generator speed	without	0.53(pu)	2%	STATCOM
			with	0.55(pu)		
2. External circuit	Combined from external circuit, current, and voltage controllers	Relative to generator fault current	without	0.68(pu)	2%	STATCOM
			with	0.70(pu)		

The following conclusions can be drawn from the results presented in Table 4.4:

1. The comparison shows that the RSC controller for both methods has been modified and combines three different controllers. The difference, in this thesis, is that an

alternative external circuit is used to support grid voltage instead of the electromagnetic torque controller.

2. This comparison clarifies that the methodology used in the first method to support the grid voltage is relative to the generator speed. However, in this work, the methodology to support the grid depends on the generator fault current.
3. This comparison indicates that the two methods have the same improvement in FRT capability of the wind turbine-based DFIG with 2% during a grid fault.

Consequently, it can be observed that improvements to the FRT capability of the DFIG including voltage support achieved by [9] can also be obtained by the proposed external circuit.

This technique has advantages since using current as a feedback, so the variable is less complex that using the electromagnetic torque method.

Furthermore, the proposed method supports the voltage by 0.02 (pu), meaning 15% of the rated voltage 1(pu). Therefore, the proposed method successfully satisfied grid code requirements which requests an FRT capability of up to 15 % of retaining voltage [14].

In this thesis, STATCOM is the only reactive power source used to support grid voltage. The unique point is to take advantage of the DFIG during a fault when switching to over-excited mode to support the reactive power. At this particular moment, the ΔV_{ref} is applied to adjust the reference voltages of the STATCOM and RSC controllers. On the other hand, the high cost of using STATCOM may be considered a disadvantage.

4.4 SUMMARY

In this chapter, improvements to the FRT capability of the DFIG during grid fault were tested and confirmed on a wind turbine, and the objective (namely, the reduction of the

voltage drop peak during grid fault) was obtained with the proposed external circuit. Furthermore, the FRT issue was initially improved at a specific point on the transmission lines and then improved at PCC. The impact of the crowbar was also discussed. A comparison with other methods shows that the proposed method has achieved the same results in voltage support at DFIG terminals.

CHAPTER 5 CONCLUSION AND FUTURE WORK

5.1 CONCLUSION

Overcoming limitations and issues related to the FRT capability of the DFIG is currently a prime topic of research, and many techniques have been proposed in this area. In this present work, the FRT issue was enhanced by using the proposed external circuit. Earlier in the thesis, the aerodynamic model of a wind turbine was discussed and analyzed because it is required for simulating FRT capability during grid faults, as are the mechanical and electrical components presented in this thesis. Currently, due to increased implementation of wind turbines, most system operators demand that a wind turbine supply reactive power during a fault in order to support the voltage recovery. For a fixed wind turbine, there are numerous options for fulfilling the requirements of reactive power, the best one of which uses FACTS controllers. However, for a DFIG coupled to a wind turbine, this compensation can be achieved with the assistance of a back-to-back converter as well FACTS controllers. Consequently, the RSC controller is modified in this study to support the grid voltage and improve FRT capability during a fault.

An external circuit was applied to a DFIG-based wind turbine connected to a power system. This was then validated by improving the FRT at the PCC and DFIG terminals during a grid fault, clearly demonstrating the efficacy of the proposed method, as the external circuit successfully improved the FRT. The impact of the crowbar protection method on FRT was also discussed and compared with the external circuit method.

The capability of the external circuit to improve voltage support during a fault has been affirmed and compared to similar methods. According to the results obtained, it can

be concluded that a proper setting of the external circuit, including the controllers, may be integrated to the RSC controller of the DFIG to achieve results that are equivalent to those created by an electromagnetic torque controller applied to an RSC controller.

The literature review in this thesis demonstrated the current and past methods used to address and resolve issues related to FRT capability of DFIG wind turbines. The focus of this thesis was thus how to improve the FRT in light of the issues discussed in the review.

5.2 FUTURE WORK

The area of study encompassed by this thesis and the solutions and methods explored in this work can be further expanded to further research areas, as per the following suggestions:

- The issue of FRT capability of DFIGs during grid faults can be reconsidered using alternative combination approaches, such as united power flow controllers (UPFC) and other reactive power sources.
- The management of reactive power from wind farm providers could be considered a non-liner optimization problem. Hence, an optimization method such as modified bacterial foraging algorithm (MBFA) could be used to solve this task.
- The performance of the external circuit presented in this thesis can be compared with other techniques.

REFERENCES

[1] B. Chitti Babu, and K.B.Mohanty. "Doubly-fed induction generator for variable speed wind energy conversion systems-modeling & simulation." International Journal of Computer and Electrical Engineering, vol. 2, no. 1, pp. 1793-8163, 2010.

[2] Siret, "The wind turbines and wind farms database." Internet: http://www.thewindpower.net/index.php, Sep.2012 [Oct.2012]

[3] Simoes, M. Godoy, and Felix A. Farret. Renewable energy systems. 2004:CRC.

[4] S. Muller, M. Deicke and R. W. De Doncker. "Doubly fed induction generator systems for wind turbines." Industry Applications Magazine, IEEE, vol. 8, no. 3, pp. 26-33, 2002.

[5] J. B. Ekanayake, L. Holdsworth and N. Jenkins." Comparison of 5th order and 3rd order machine models for doubly fed induction generator (DFIG) wind turbines." Electr. Power Syst. Res, vol. 67, no. 3, pp. 207-215,2003.

[6] Staff of lab-volt, "Principles of doubly-fed induction generator," Lab-volt electric power technology training program, Canada, Tech. Rep. 86376-F0. 2011.

[7] Jia, X., Tian L., Xing Z. X., Su X. B., "Dynamic Model and Simalation of Double Feed Induction Generator Wind Turbine," IEEE International Conferences on Automation and Logistics, pp.1667-1671, 2009.

[8] A. D. Hansen and G. Michalke. "Fault ride-through capability of DFIG wind turbines." Renewable Energy, vol. 32, no. 9, pp. 1594-1610, 2007.

[9] K. Ahsanullah and J. Ravishankar, "Fault ride-through of doubly-fed induction generators," in Proc. of Int. Conference on Power, Signals, Controls and Computation (EPSCICON), 2012, pp. 1-6.

[10] G. Abad, J. Lop'ez, M. Rodriguez, L. Marroyo and G. Iwanski. Doubly Fed Induction Machine Modeling and Control for Wind Energy Generation. Hoboken,New Jersey: John wiley&sons, 2011.

[11] M. Wilch, V.S. Pappala, S.N. Singh, I. Erlich. "Reactive power generation by dfig based wind farms with ac grid connection," Power Tech, 2007, IEEE, Lausanne (2007), pp. 626‑632.

[12] M.Seyedi. "Evaluation of the DFIG wind Turbine Built-in Model in PSS/E,"M.A.thesis, Chalmers University of Technology, Sweden, 2009.

[13] S. Seman , J. Niiranen , S. Kanerva , A. Arkkio and J. Saitz. "Performance study of a double fed wind-power induction generator under network disturbances." IEEE Transactions. Energy Conversion, vol. 21, no. 4, pp. 883 -890, 2006.

[14] A. Dittrich and A. Stoev. "Comparison of fault ride-through for wind turbines with DFIM generators," in proc. 11th Eur. Conf. Power Electron. Appl., pp. 1 -8, 2005.

[15] L. Zhang, X. Jin and L. Zhan. "Reactive power control of doubly fed induction generator during grid voltage dips," in proc.APPEEC 2012 Power and Energy Engineering Conference , 2012.

[16] S. Seman, J. Niiranen and A. Arkkio. "Ride-through analysis of doubly fed induction wind-power generator under unsymmetrical network disturbance." Power Systems, IEEE Transactions, vol. 21, no 4, pp. 1782-1789, 2006.

[17] Dawei Xiang, Li Ran, P. J. Tavner and S. Yang. "Control of a doubly fed induction generator in a wind turbine during grid fault ride-through." Energy Conversion, IEEE Transactions, vol. 21,no. 3, pp. 652-662, 2006.

[18] Jin Yang, J. E. Fletcher and J. O'Reilly. "A series-dynamic-resistor-based converter protection scheme for doubly-fed induction generator during various fault conditions." Energy Conversion, IEEE Transactions, vol. 25, no.2 , pp. 422-432,2010.

[19] B. Gong, D. Xu and B. Wu. "Cost effective method for DFIG fault ride-through during symmetrical voltage dip,"in proc.IECON 2010,36th Annual Conference on IEEE Industrial Electronics Society, pp. 3269-3274, 2010.

[20] C. Zhan and C. D. Barker. "Fault ride-through capability investigation of a doubly-fed induction generator with an additional series-connected voltage source converter. Presented at AC and DC Power Transmission,"in proc.ACDC 2006, 8th IEE International Conference , pp.79 -84, 2006.

[21] J. Morneau, C. Abbey and G. Joos." Effect of low voltage ride through technologies on wind farm,"in proc.Electrical Power Conference, 2007. EPC 2007. IEEE Canada, pp.56 -61 ,2007 .

[22] N. Joshi and N. Mohan. "A novel scheme to connect wind turbines to the power grid. Energy Conversion," IEEE Transactions, vol.24, no.2, pp. 504-510,2009.

[23] S. Santoso and H. T. Le. "Fundamental time–domain wind turbine models for wind power studies," Renewable Energy, vol. 32,no. 14, pp. 2436-2452. 2007.

[24] Heier, Siegfried. Grid integration of wind energy conversion systems. Hoboken: Wiley, 1998.

[25] Patel, Mukund R. Wind and solar power systems: design, analysis, and operation. CRC, 2005.

[26] "Wind turbine implement model of variable pitch wind turbine." Internet: Http://www. Mathworks. Com.

[27] J. G. Slootweg, H. Polinder and W. L. Kling. "Dynamic modelling of a wind turbine with doubly fed induction generator," in proc. Power Engineering Society Summer Meeting, 2001.

[28] H. H. Aly and M. E. El-Hawary. "An overview of offshore wind electric energy resources," in proc. Electrical and Computer Engineering (CCECE), 2010 23rd Canadian Conference ,2010.

[29] F. Mei and B. C. Pal. "Modelling and small-signal analysis of a grid connected doubly-fed induction generator," in proc. Power Engineering Society General Meeting, 2005. IEEE, pp.358 -367 ,2005.

[30] F. Iov, A.D. Hansen, P. Sørensen and F. Blaabjerg, "Wind Turbine Blockset in Matlab/Simulink. General Overview and Description of the Models", Aalborg University, March 2004, ISBN 87-89179-46-3.

[31] J. B. Ekanayake, L. Holdsworth, X. G. Wu and N. Jenkins. "Dynamic modeling of doubly fed induction generator wind turbines," Power Systems, IEEE Transactions,vol. 18,no. 2,pp. 803-809. 2003.

[32] J. B. Ekanayake, L. Holdsworth and N. Jenkins. "Comparison of 5th order and 3rd order machine models for doubly fed induction generator (DFIG) wind turbines," Electr. Power Syst. Res. vol. 67,no. 3, pp. 207-215. 2003.

[33] B. Dosijanoski. "Simulation of Doubly-Fed Induction Generator in a Wind Turbine, " in proc. XI International PhD Workshop,OWD 2009, pp. 378-383,2009.

[34] H. Camille. "Doubly-fed Induction Generator Modeling and Control in DigSilent Power Factory," M.A. thesis, KTH School of Electrical Engineering, 2010.

[35] M. Milosevic. "Decoupling Control of d and q Current Components in Three-Phase Voltage Source Inverter," Technical Report, 2003.

[36] E.on Netz Grid Code,"High and extra high voltage." Internet: http://www.pvupscale.org/IMG/pdf/D4_2_DE_annex_A3_EON_HV_grid__connection_requirements_ENENARHS2006de.pdf , 2006.

[37] H.Markiewicz and A.Klajn . " Voltage Disturbances Standard EN 50160 -Voltage Characteristics in Public Distribution Systems," Technical Report, 2004.

[38]http://www.mathworks.com/help/physmod/powersys/ref/staticsynchronouscompensatorphasortype.html

[39]http://www.mathworks.com/help/physmod/powersys/ug/wind-farm-using-doubly-fed-induction-generators.html

[40]http://www.mathworks.com/help/physmod/powersys/ref/windturbinedoublyfedinductiongeneratorphasortype.html

APPENDIX A

The following MATLAB code was used to draw the performance coefficient(c_p) as a function of tip speed ratio (λ) with pitch angle (β) as parameter in addition to extract the c_p (base) and λ (base) when $\beta = 0$

```
B=0;
for m=1:15
H(m)=1/(m+0.08*B)-0.035/(B*B*B+1);
l(m)=1/H(m);


cp(m)=0.5176*(116/l(m)-0.4*B-5)*exp(-21/l(m))+0.0068*m;
end
m=[1:1:15];
plot(m,cp(m));
grid
 [cpmax,mmx]=max(cp(m))
 xlabel('Tip speed ratio lmbdas')
ylabel(' Performance coefficient cp')
text(7,0.55,'0 deg')


B=2;
for m=1:15
H(m)=1/(m+0.08*B)-0.035/(B*B*B+1);
l(m)=1/H(m);


cp(m)=0.5176*(116/l(m)-0.4*B-5)*exp(-21/l(m))+0.0068*m;
end
m=[1:1:15];
hold on
plot(m,cp(m));
text(10.2,0.49 ,'{2 deg}')

B=5;
for m=1:15
H(m)=1/(m+0.08*B)-0.035/(B*B*B+1);
l(m)=1/H(m);


cp(m)=0.5176*(116/l(m)-0.4*B-5)*exp(-21/l(m))+0.0068*m;
end
```

```
m=[1:1:15];
hold on
plot(m,cp(m));
text(13.2,0.3 ,'{5 deg}')



B=10;
for m=1:15
H(m)=1/(m+0.08*B)-0.035/(B*B*B+1);
l(m)=1/H(m);


cp(m)=0.5176*(116/l(m)-0.4*B-5)*exp(-21/l(m))+0.0068*m;
end
m=[1:1:15];
hold on
plot(m,cp(m));
text(8,0.3 ,'{10 deg}')


B=15;
for m=1:15
H(m)=1/(m+0.08*B)-0.035/(B*B*B+1);
l(m)=1/H(m);


cp(m)=0.5176*(116/l(m)-0.4*B-5)*exp(-21/l(m))+0.0068*m;
end
m=[1:1:15];
hold on
plot(m,cp(m));
text(8,0.17 ,'{15 deg}')


B=20;
for m=1:15
H(m)=1/(m+0.08*B)-0.035/(B*B*B+1);
l(m)=1/H(m);


cp(m)=0.5176*(116/l(m)-0.4*B-5)*exp(-21/l(m))+0.0068*m;
end
m=[1:1:15];
hold on
plot(m,cp(m));
text(7,0.1 ,'{20 deg}')
```

APPENDIX B

Table (C1) A wind turbine and power transmission system Data are below

Wind Turbine Data	
Base mechanical power(P_{mech})	$6.5 \times 1.5\text{MW} = 9\text{MW}$
The wind speed	12m/s
Power Transmission System Data	
Bus bare (B1)	575(V)
Bus bare (B2)	25(KV)
Bus bare (B3)	25(KV)
Bus bare (B4)	120(KV)
Bus bare of point of common coupling (PCC)	120(KV)
Load	500(KW)
Plant	2(MVA)
Transformer 1 Y, Δ	25KV/575V, 12(MVA)
Transformer 2 Y, Δ	120KV/25KV, 47(MVA)
Line 1	10(Km)
Line 2	40(Km)
Grid	120(KV), 60(Hz)
Grid equivalent reactance	Zero sequence parameters/positive sequence parameters=3

Table (C2) A DFIG, parameters of RSC controller and parameters of GSC controller Data.

DFIG Data	
Base power (s)	$1.5 \times 10^6/_{0.9}$ (VAR)
Base line to line voltage	575 (V)
The stator resistance in per unit (R_s)	0.00706 (pu)
The stator inductance in per unit (L_s)	0.171(pu)

The rotor resistance in per unit (R_r)	0.005(pu)	
The rotor inductance in per unit (L_r)	0.156(pu)	
The mutual inductance in per unit(L_m)	2.9(pu)	
Base Frequency	60 (Hz)	
The number of the poles (p)	3	
Inertia constant	5.04	
Fraction	0.01	
Parameters of RSC controller Data		
	K_p	K_i
voltage regulator	1.5	300
Power regulator	1	100
Current regulator	0.3	8
Parameters of GSC controller Data		
	K_p	K_i
Dc –voltage regulator	0.002	0.05
Current regulator	1	100
Droop (X_s)	0.02(pu)	

Table (C3) An external circuit Data.

	K_p	K_i
Generator side regulator	70	14
STATCOM side regulator	0.316	1e-004
Critical value	0.9(pu)	
STATCOM	100(MAV)	
The impedance type factor (γ)	0.2(pu)	